

NASA CR 97716

NATIONAL AERONAUTICS AND SPACE ADMINISTRATION

CASE FILE
COPY *Technical Report 32-1300*

*Radio-Frequency Performance of an 85-ft
Ground Antenna: X-Band*

Dan A. Bathker

JET PROPULSION LABORATORY
CALIFORNIA INSTITUTE OF TECHNOLOGY
PASADENA, CALIFORNIA

July 1, 1968

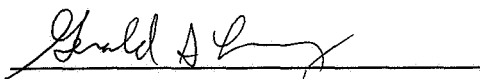
NATIONAL AERONAUTICS AND SPACE ADMINISTRATION

Technical Report 32-1300

*Radio-Frequency Performance of an 85-ft
Ground Antenna: X-Band*

Dan A. Bathker

Approved by:

A handwritten signature in dark ink, appearing to read "Gerald S. Levy", is written over a horizontal line.

Gerald S. Levy, Manager
Communications Elements Research Section

JET PROPULSION LABORATORY
CALIFORNIA INSTITUTE OF TECHNOLOGY
PASADENA, CALIFORNIA

July 1, 1968

TECHNICAL REPORT 32-1300

Copyright © 1968

**Jet Propulsion Laboratory
California Institute of Technology**

**Prepared Under Contract No. NAS 7-100
National Aeronautics & Space Administration**

Acknowledgment

The X-band evaluation program drew upon the expert assistance of many individuals. R. Stevens, P. Potter, and G. Levy suggested and supported the work. Dr. A. Moffett of the California Institute of Technology graciously advised on many occasions. T. Otschi, B. Seidel, and C. Stelzried provided the noise instrumentation, calibrations, and advice on radio astronomical methods.

S. Petty, R. Clauss, and E. Wiebe delivered, as usual, an outstanding TWM/CCR exhibiting 100% reliability. R. Gosline designed the wide dynamic range digital pattern recording system. F. McCrea completed the large aperture gain standard horn development program with excellent results. H. Reilly, Jr., was cognizant of fabricating and testing microwave feed components, as well as complete construction of the XCE feedcone on a constrained time scale. D. Nixon and P. Parsons efficiently handled the machine-reduced experimental data.

F. Stoller and W. Kissane obtained the structural field data which went a long way towards explaining the RF results. M. S. Katow provided the STAIR computed results and was instrumental in keeping structural computations in proper perspective.

A. Ludwig's original work on predicting aperture efficiency was heavily drawn upon, as was his general advice.

The Bendix Field Engineering team at the Venus Deep Space Station deserves special mention for their 24-h/day operations support.

Contents

I. Introduction	1
II. System Description	1
A. Feedcone	1
B. Feed System	3
C. Radiometer	8
III. Source Selection and Radiometric Technique	10
A. Radio Astronomical	10
B. Collimation Tower	11
1. Range requirements	11
2. Power measurement	13
3. Gain standard horn measurement	15
IV. Initial Measurements, November 1966	21
V. Supporting Studies	21
VI. Final Measurements, June 1967	24
A. Radio Astronomical	24
B. Ground Based	28
VII. Conclusion	32
References	33

Tables

1. Computed 8448-MHz feed efficiency, 85-ft antenna.	8
2. Computed 8448-MHz quadripod efficiency,, 85-ft antenna, DSS-13.	8
3. Maser performance at 8448 MHz	10
4. Power meter test for thermoelectric effect	14
5. Power meter test: smoothed and single test comparison	14
6. Power meter test for linearity	15
7. Power meter test for drift	15
8. Field data: 85-ft az-el surface tolerance	22

Contents (contd)

Tables (contd)

9. Computed data: 85-ft az-el best fit focal lengths	22
10. Computed data: 85-ft az-el rms of one-half RF pathlengths	22
11. Measured off-source system noise temperatures, 8448 MHz, DSS-13 XCE feedcone	29
12. Measured and computed parameters, ground-based gain measurement	29
13. Effective system surface tolerance computation	30
14. Independent methods of efficiency determination	32

Figures

1. X-Band cassegrain experimental (XCE) feedcone	2
2. XCE feedcone interior	3
3. Radiation pattern, XCE feed, E-plane	4
4. Radiation pattern, XCE feed, H-plane	5
5. Radiation pattern, XCE feed, 45-deg-plane	6
6. Subreflector configuration, 85-ft antenna	7
7. Subreflector scattered radiation patterns, E- and H-planes, amplitude, 85-ft antenna, 8448 MHz	7
8. Subreflector scattered radiation patterns, E- and H-planes, phase, 85-ft antenna, 8448 MHz	8
9. Block diagram of total power radiometer	9
10. Path profile, Tiefert Mountain to Venus station	12
11. Tiefert Mountain transmitter equipment	13
12. Radiation pattern, large aperture gain standard horn, E-plane	16
13. Radiation pattern, large aperture gain standard horn, H-plane	17
14. Radiation pattern, large aperture gain standard horn, 45-deg-plane	18
15. Large aperture gain standard horn pattern test range	19
16. Large aperture gain standard horn at Tiefert Mountain	19
17. XCE feedcone installed on Venus station az-el reflector	20
18. Computed surface contour map, 85-ft az-el reflector	23

Contents (contd)

Figures (contd)

19. Computed azimuth patterns, 85-ft az-el reflector, 8448 MHz	24
20. Computed elevation patterns, 85-ft az-el reflector, 8448 MHz	24
21. Cygnus A focusing as a function of elevation angle, 85-ft az-el reflector, X-band	25
22. Elevation offsets as a function of elevation angle, 85-ft az-el reflector, X-band, June 1967	26
23. Excess system temperature referenced to maser input flange, Cygnus A	27
24. Off-source system temperature referenced to maser input flange	28
25. Polynomial curve fit computation for radiation patterns	30
26. Polynomial curve for radiation patterns	30
27. Radiation pattern, 85-ft az-el reflector, near-field focus, azimuth	31
28. Radiation pattern, 85-ft az-el reflector, near-field focus, elevation	31
29. Radiation pattern, 85-ft az-el reflector, near-field source at horizon, focused for high-elevation-angle peak gain, azimuth	31
30. Radiation pattern, 85-ft az-el reflector, near-field source at horizon, focused for high-elevation-angle peak gain, elevation	31
31. Surface efficiency as a function of surface tolerance, 8448 MHz	32

Abstract

The NASA/JPL Deep Space Instrumentation Facility 85- and 210-ft paraboloidal ground antennas have previously been demonstrated to operate well below gain limit at S-band. The results of approximately 6 weeks' experimental effort together with supporting studies of an 85-ft paraboloid at X-band are given. Determinations of the aperture efficiency by independent methods are in close agreement and show the system remains below gain limit at X-band. Mechanical perturbations including ordered changes in the paraboloid focal length were evaluated by radio-frequency and machine-reduced field data obtained by civil engineering techniques.

Radio-Frequency Performance of an 85-ft Ground Antenna: X-Band

I. Introduction

The gain of a phase-error-free aperture-type antenna is proportional to the frequency squared; however, several physical effects cause phase errors in the aperture of any realizable structure. When the frequency rate of change of gain loss due to phase errors is equal and opposite to the frequency-squared law, the antenna is said to be at gain limit. Operating a large ground antenna for purposes of deep space communications near, or at, gain limit is advantageous for certain restricted cases depending on the type of link, frequency, and spacecraft technology (Ref. 1). Under these conditions, detailed knowledge of the behavior of the ground antenna structure becomes important since the radio-frequency performance is a sensitive function of mechanical perturbations.

Previous evaluations of NASA/JPL Deep Space Instrumentation Facility (DSIF) 85- and 210-ft paraboloidal reflectors have shown both systems are clearly well below gain limit at S-band, 2300 MHz. In this report the results of approximately 6 weeks' experimental effort together with supporting studies of an 85-ft paraboloid at X-band are given. A reasonably clear picture of the po-

tentials of this aperture/frequency relationship has been obtained; the results show the work was conducted, for all conditions encountered, at less than 0.6 times gain limit frequency.

II. System Description

A. Feedcone

The DSIF 85- and 210-ft antennas employ cassegrain RF optics in which the primary feed, preamplifier, and calibration equipment are housed within a standard support cone. This arrangement, which has proven operationally convenient in the field and has given the ability to perform system checkouts using the feedcone on the ground, was retained in the X-band cassegrain experimental (XCE) feedcone (Fig. 1). This feedcone was constructed during 1966 for the antenna evaluation program at X-band, 8448 MHz. The XCE feedcone is fitted with equipment appropriate for the evaluation task: a traveling wave maser preamplifier and total power radiometer for observations of a few celestial sources and a separate crystal mixer front end for ground-based collimation tower work. Figure 2 shows the feedcone interior.

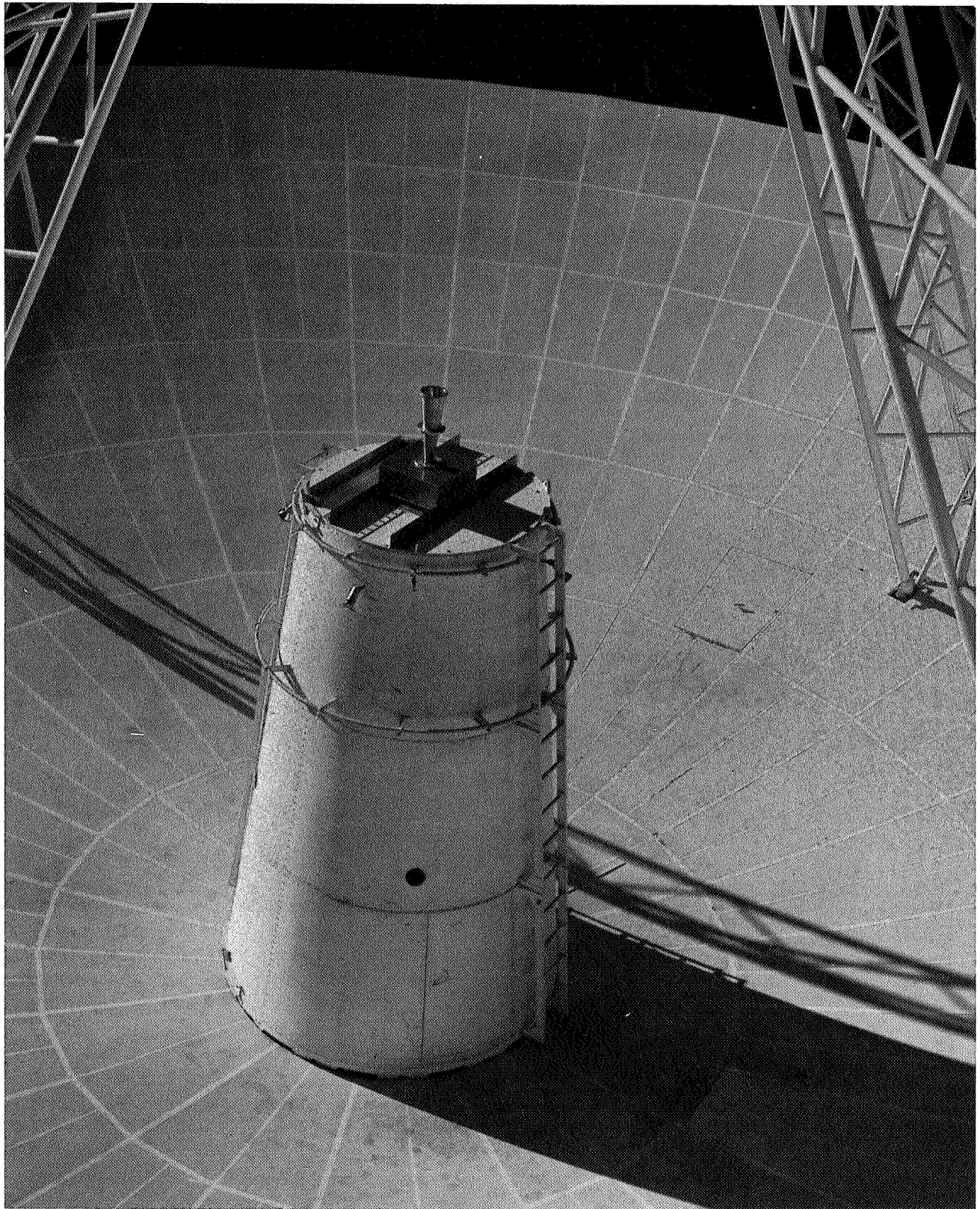


Fig. 1. X-band cassegrain experimental (XCE) feedcone



Fig. 2. XCE feedcone interior

B. Feed System

The feed is a scale model of the high-performance Venus radar feed (Ref. 2) with the turnstile junction polarizer and the mode generator fabricated of OFHC copper. Wherever possible, heavy wall (0.125 in.) OFHC copper WR 112 waveguide is used with flanging accomplished with thick (0.50 in.) CPR-112 dowel pinned flanges.

Figures 3-5 show the feedhorn 8448-MHz E-, H-, and 45-deg-plane radiation patterns. Figure 6 gives the feed geometry used on the 85-ft antennas, including the beam-shaping flange that is nominally 2λ wide at S-band. The

Rusch scattering program (Refs. 3 and 4) was used to obtain the 8448-MHz radiation patterns of the cassegrain system. Figures 7 and 8 show the slight pattern distortion occurring near the edge of the paraboloid (illumination angle = 61 deg) caused by the large wavelength-sized flange.

Aperture integration methods developed by Ludwig (Ref. 5) were used to evaluate the feed system. Table 1 gives the components considered and the overall feed system efficiency. An estimated 3σ tolerance somewhat in excess of 0.5% has been assigned to the evaluation. Although the large wavelength-sized flange degrades the system a small amount, the convenience of retaining

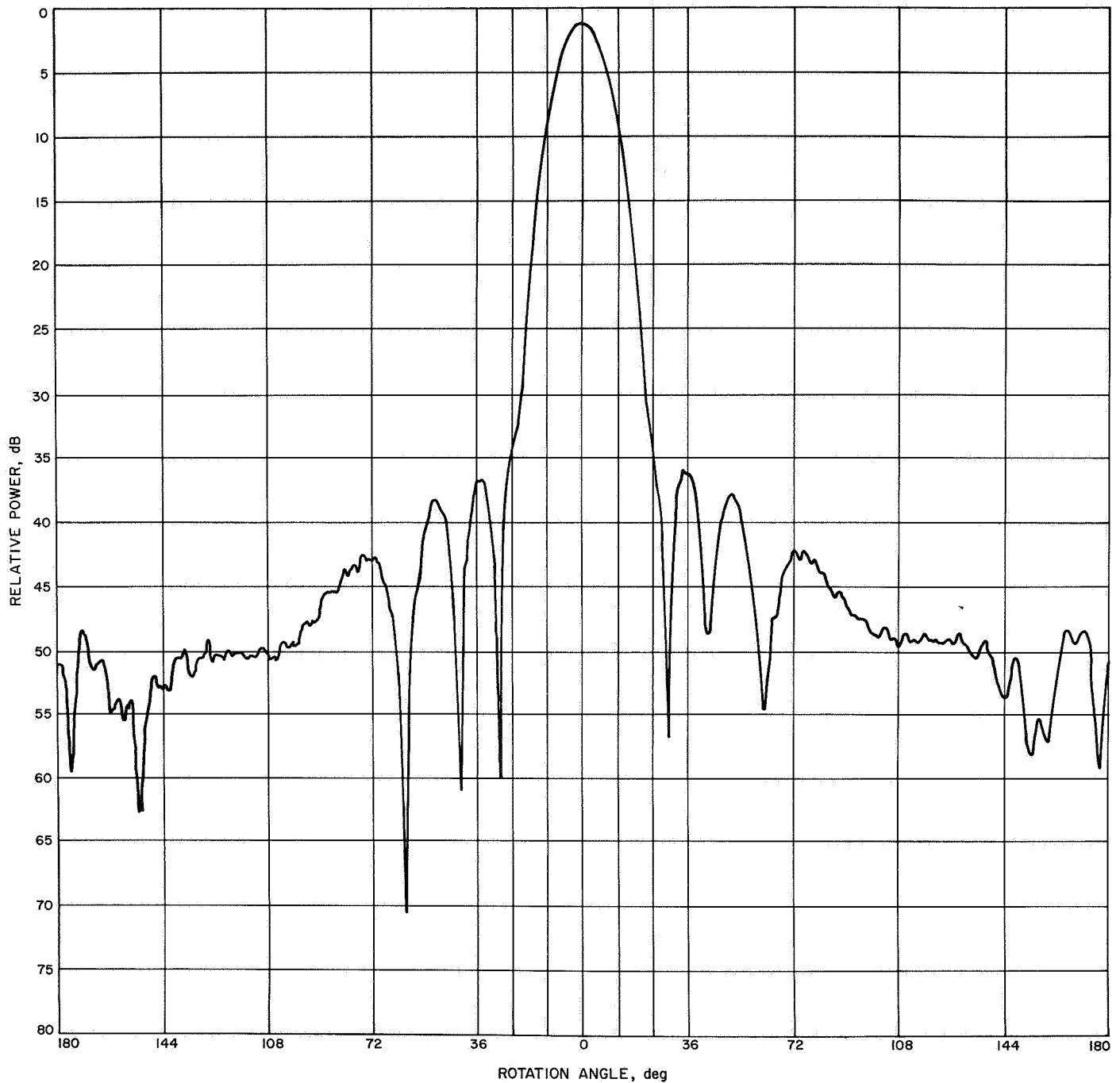


Fig. 3. Radiation pattern, XCE feed, E-plane

the S-band flange during intermittent X-band work was a distinct benefit. The normally used S-band vertex matching plate was removed for both the above calculations and the experimental work. While the feed evaluation method outlined above makes use of the linear polarization characteristics of the feed, the system is normally operated in the right hand circular polarization

(RCP) mode. During the feed system tests, the polarizer was adjusted to obtain 0.30-dB ellipticity.

An optical analysis of the 85-ft antenna quadripod structure to be used shows the structure blocks 6.43% of the available aperture. Assuming the percentage of intercepted energy equals the percentage of area, which

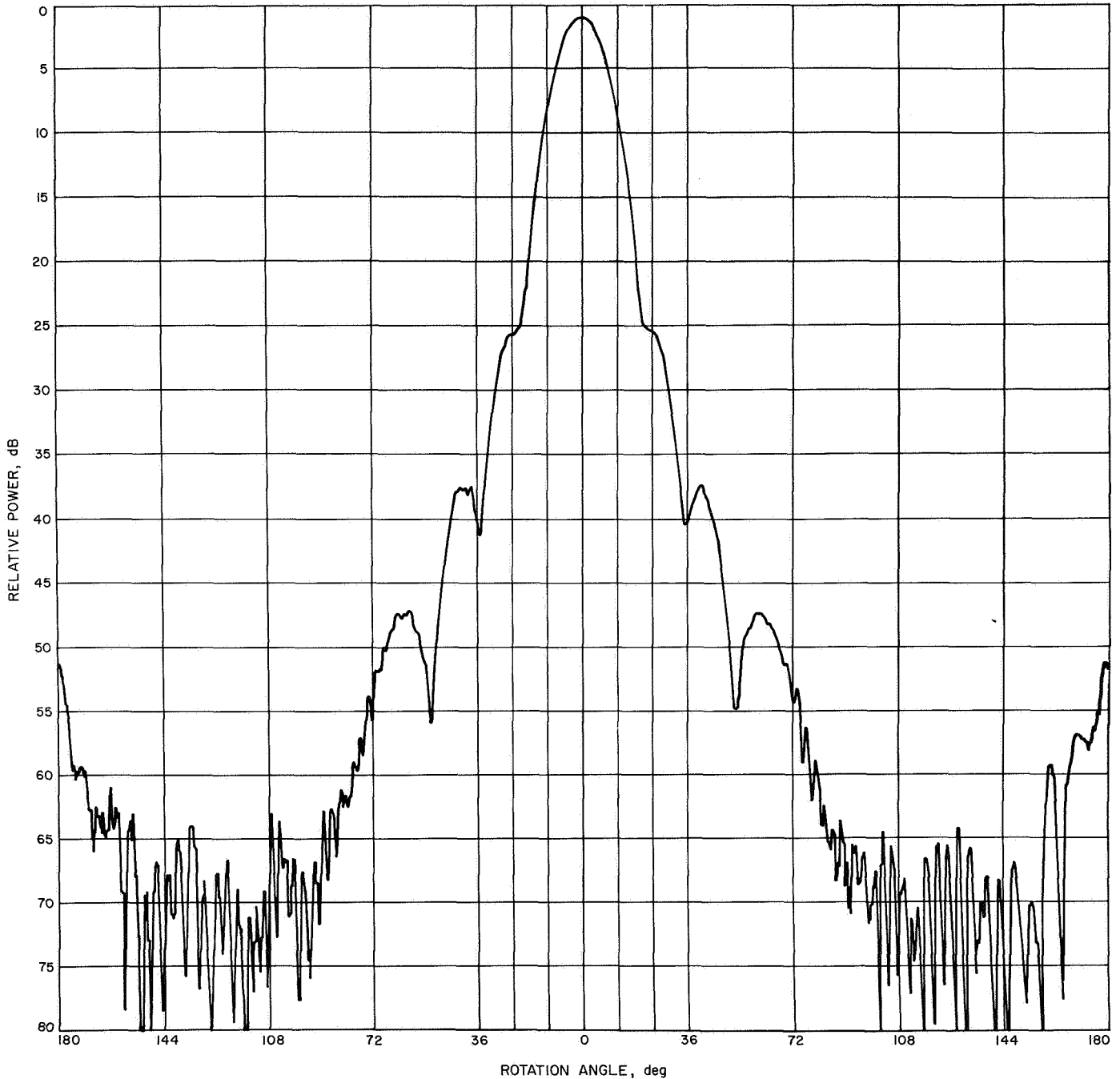


Fig. 4. Radiation pattern, XCE feed, H-plane

constitutes accepting pie-slice approximations of the blocked areas in the aperture, it has been shown (Ref. 6) that

$$\eta' = \eta (1 - B)^2 \quad (1)$$

where η'/η is the loss due to blocking, and B is the fractional area blocked. Actually, $B = \sigma A$, where σ is defined

as an average RF opacity and A is the optically blocked area. Because of the large wavelength size of the quadripod cross section at X-band, the opacity is estimated to be $0.8 < \sigma < 1.2$.

Table 2 gives the components considered and the overall quadripod blockage efficiency, assuming the estimated opacities represent 3σ limits.

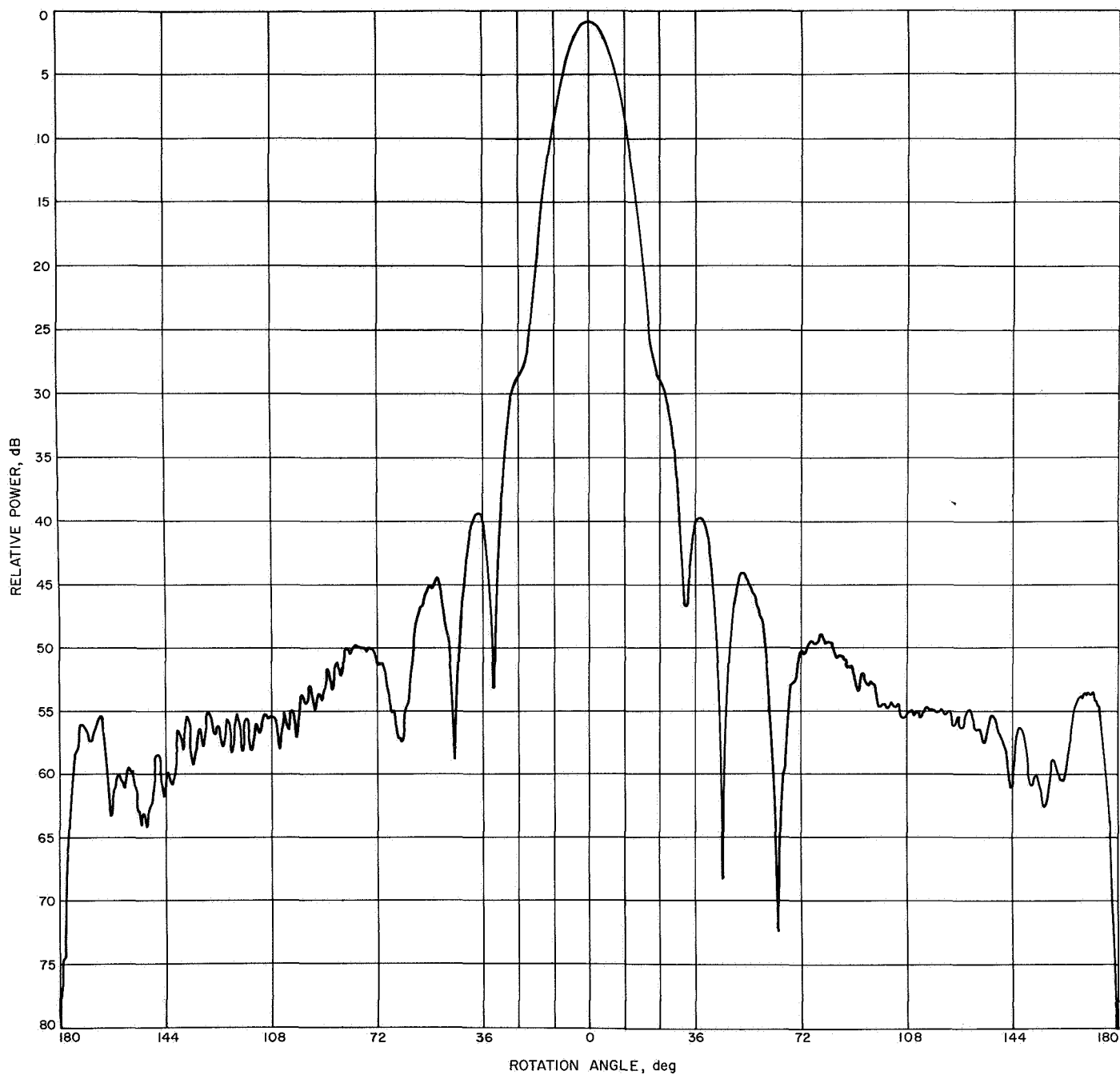


Fig. 5. Radiation pattern, XCE feed, 45-deg-plane

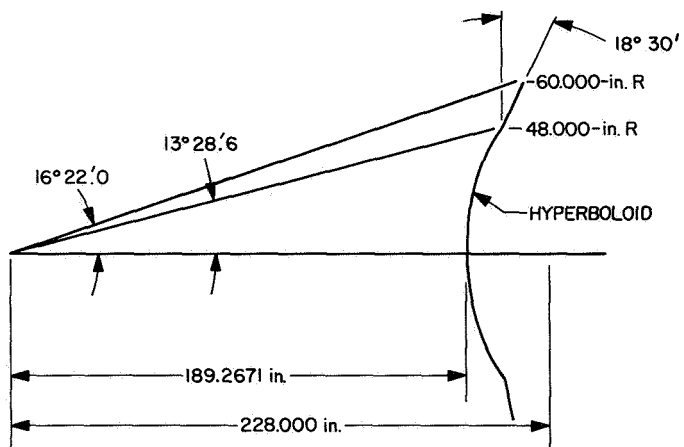


Fig. 6. Subreflector configuration, 85-ft antenna

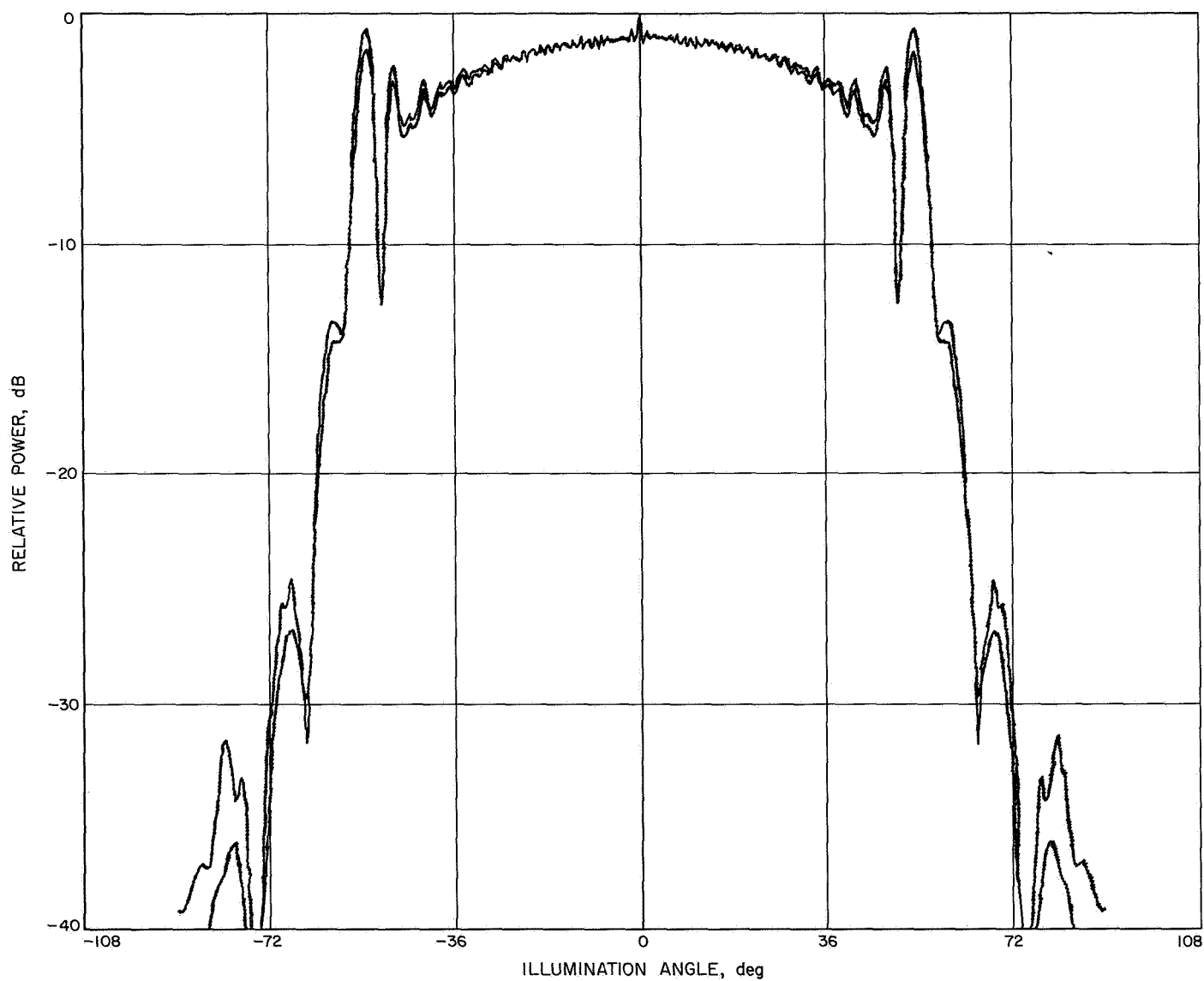


Fig. 7. Subreflector scattered radiation patterns, E- and H-planes, amplitude, 85-ft antenna, 8448 MHz

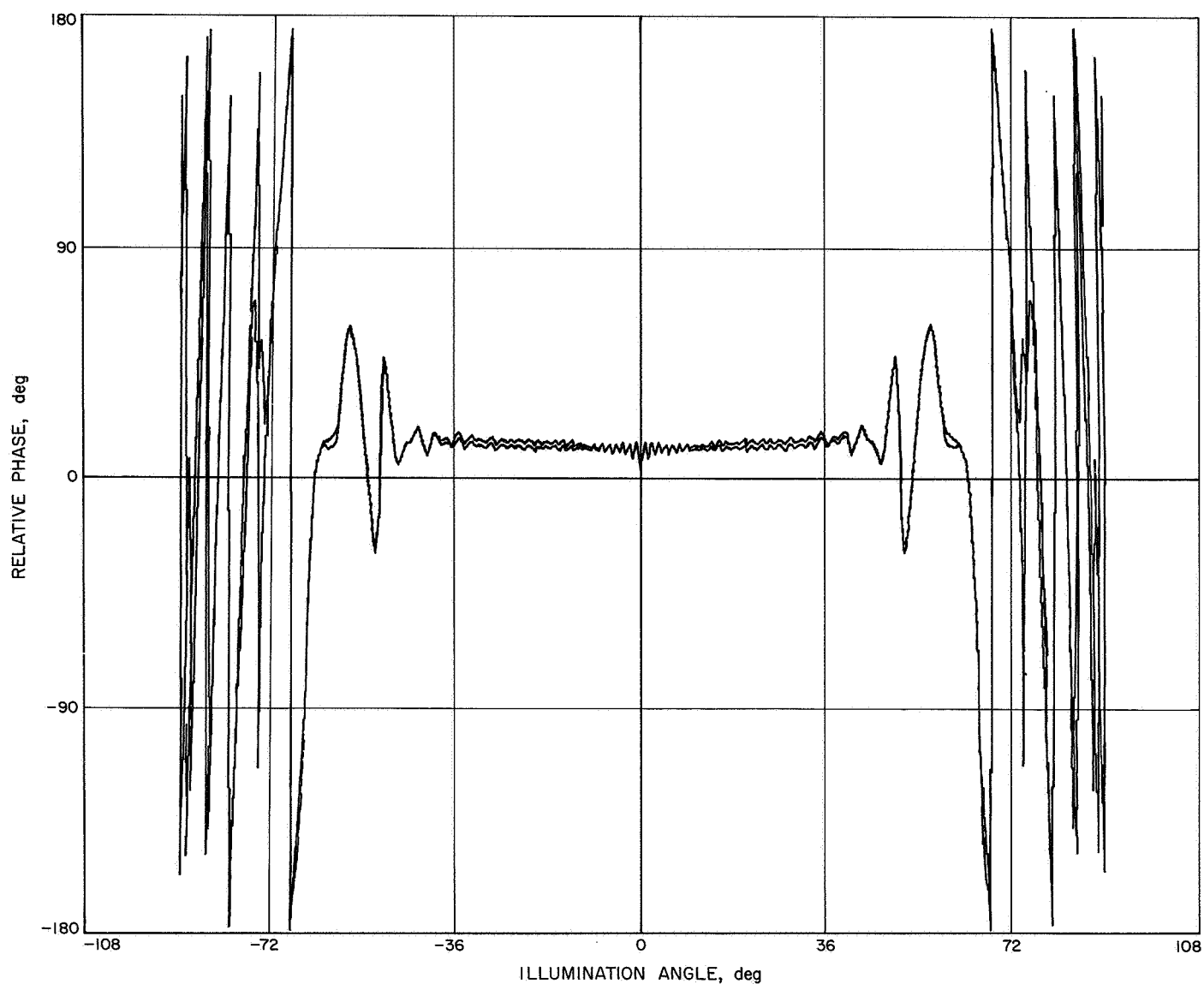


Fig. 8. Subreflector scattered radiation patterns, E- and H-planes, phase, 85-ft antenna, 8448 MHz

**Table 1. Computed 8448-MHz feed efficiency
85-ft antenna**

Parameter	Value
Forward spillover	0.0406
Rear spillover	0.0039
Illumination efficiency	0.8526
Cross polarization efficiency	0.9993
Phase efficiency	0.9406
Subreflector blockage efficiency	0.9647
Overall feed efficiency	$0.7388 \pm 0.002, 1\sigma, \text{ est.}$

**Table 2. Computed 8448-MHz quadripod efficiency
85-ft antenna, DSS-13**

Parameter	Value
Blocked Area A	0.0643
Opacity σ	0.80–1.20
Quadripod blockage efficiency η'/η	$0.8755 \pm 0.008, 1\sigma \text{ est.}$

C. Radiometer

Figure 9 shows the block diagram of the total power radiometer used for celestial source measurements. Not

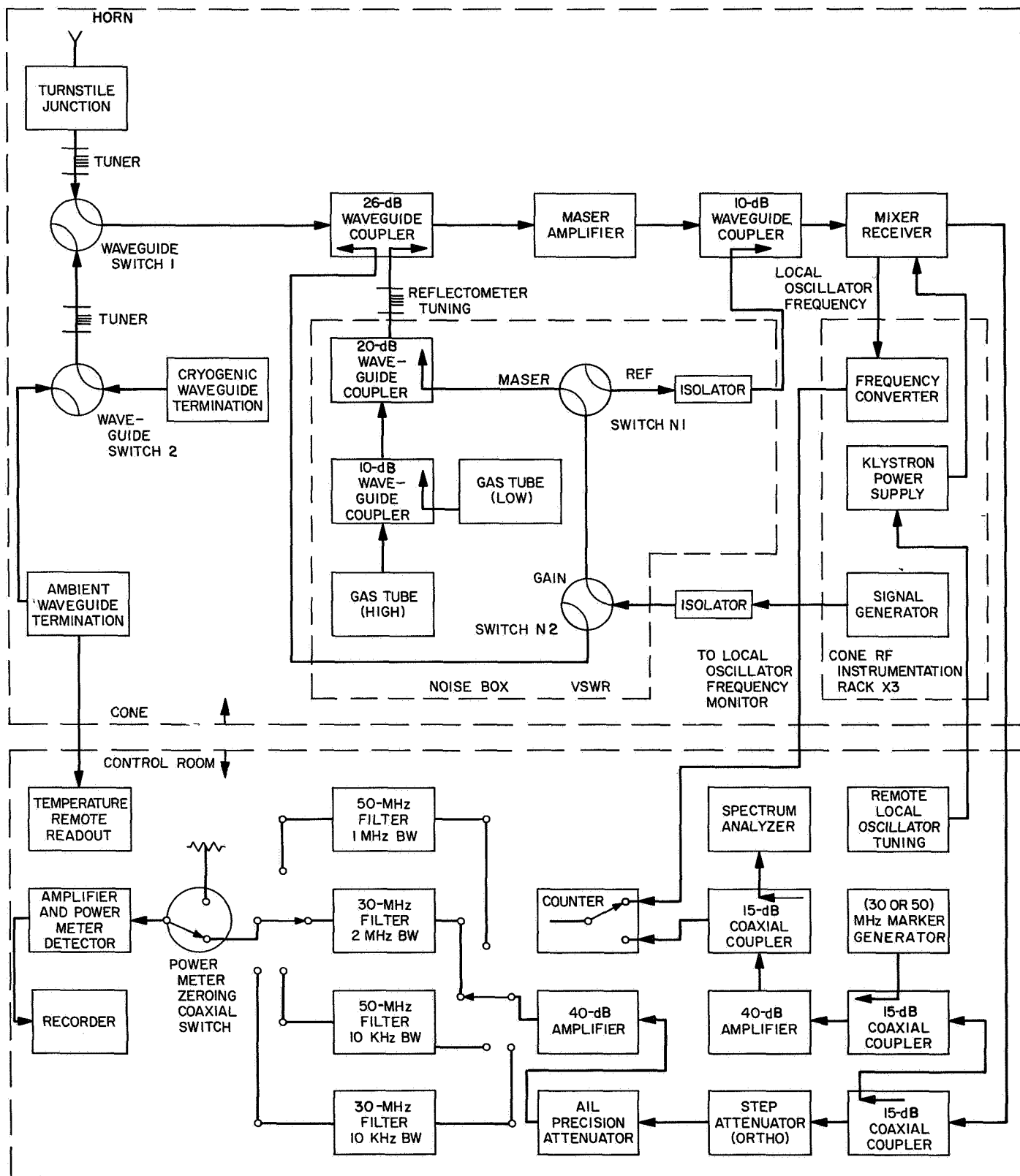


Fig. 9. Block diagram of total power radiometer

shown is the separate crystal mixer front end used for higher signal level ground-based measurements. The high-level radiometer uses the station phase-locked receiver to derive automatic gain control (AGC) indications of signal level. The AGC voltage is used to drive a voltage-to-frequency converter that feeds the station doppler equipment for recording wide-dynamic-range antenna radiation patterns.

The traveling wave maser is operated in a closed-cycle helium refrigerator and has been described in detail (Ref. 7). Briefly, the preamplifier characteristics are given in Table 3. The instrumentation allows for measurements of the antenna, ambient and cryogenic termination VSWR, and maser gain and noise temperature. The receiver local oscillator frequency is monitored, and the temperature of the ambient load is read out using a quartz thermometer. Normally, the antenna temperature calibrations are made using the ambient load-to-antenna Y-factor technique with periodic checks using the cryogenic termination. The dissipative attenuation between the antenna reference flange and the maser reference flange was measured as (0.150 ± 0.0018) dB, 3σ . Estimated turnstile junction and horn losses are 0.025 and 0.018 dB, respectively. The system was usually operated with 1 MHz bandwidth and early results (November 1966) characterized the zenith system noise contributions on an 85-ft antenna as $T'_A = 13.6^\circ\text{K}$, $T''_M = 16.1^\circ\text{K}$, $T_L = 9.5^\circ\text{K}$, and $T''_F = 0.5^\circ\text{K}$, where T_A , T_M , T_L , and T_F are the antenna, maser, loss, and followup receiver contributions, respectively. Single superscripts refer to the antenna reference flange, while double superscripts refer to the maser reference flange. Later results (June 1967) were: $T'_A = 13.0^\circ\text{K}$, $T''_M = 13.7^\circ\text{K}$, $T_L = 9.5^\circ\text{K}$, and $T''_F = 0.5^\circ\text{K}$ for a total zenith system noise temperature on an 85-ft antenna of less than 37°K .

The overall radiometer operating in a ground checkout mode has a short term (minute) resolution of 0.1°K and a peak systematic error of about 0.2°K when observing a 5°K source.

Table 3. Maser performance at 8448 MHz

Parameter	Value
Signal frequency	8448 MHz
Net gain	41.5 dB
Bandwidth (3 dB)	17 MHz
Equivalent input noise temperature	$< 18^\circ\text{K}$

III. Source Selection and Radiometric Technique

A. Radio Astronomical

A study of the literature (Ref. 8)¹ indicated Cygnus A (3C405) as the best source for the 85-ft antenna evaluation. The criteria leading to selection of Cygnus A were:

- (1) Strength. The source should be strong enough to observe without excessive integration times, and the flux density should be well known.
- (2) Declination. The source should appear high in the local sky for several reasons including reduction of atmospheric effects and to allow a wide elevation angle range of measurements.
- (3) Distribution. The source should be a point source for reliable data reduction.

The value of flux density of Cygnus A at 8448 MHz was taken to be

$$S = (187.6 \pm 28.1) \times 10^{-26} \text{ w} \cdot \text{m}^{-2} \cdot \text{Hz}^{-1} (3\sigma)$$

The change in antenna temperature, due to the flux density of a point source, is given by

$$T_a = \frac{SA}{2k} \quad (2)$$

where

T_a = the change in antenna temperature, due to the source, in $^\circ\text{K}$

S = the flux density of the source, in w/m^2 (Hz)

A = the cross-sectional area of the collecting aperture, in m^2

k = Boltzmann's constant:

$$1.3805 \times 10^{-23} \text{ w} \cdot ^\circ\text{K}^{-1} \cdot \text{Hz}^{-1}$$

Cygnus A, though not a point source, was considered to be two point sources that are separated by 100 s of arc and having relative intensities of 1.2 to 1.

Assuming the antenna beam is directed to a point between the two sources that comprise Cygnus A, and that this point is analogous to the center of moments in a two-point mass mechanical system, a small correction has to be applied to the conversion from flux density to antenna source temperature. The corrected form for the

¹Also, private communication, Dr. A. Moffett, California Institute of Technology, Pasadena, Calif.

conversion is, for the case of Cygnus A and the expected beamwidth,

$$T_a = \frac{SA}{2k} \left[\frac{(1.2)(0.95) + (1.0)(0.94)}{2.2} \right] \quad (3)$$

Substituting into this equation yields $(34 \pm 5.1)^\circ\text{K}$, (3σ) as the increase in antenna temperature due to Cygnus A for a 100% efficient, 85-ft antenna operated at 8448 MHz.

The Y-factor method of determining the increase in temperature due to the source references the measurement to the maser reference flange. Data of this kind are useful for a deep space communications system designer; i.e., several effects such as microwave dissipation loss, atmospheric extinction, and gain loss as a function of elevation angle are automatically included in the observations. By measuring the excess system temperature due to the source at the maser reference flange and comparing this to $(34 \pm 5.1)^\circ\text{K}$, we define an overall system efficiency; the system happens to include the atmosphere and other losses. Similarly, off-source system temperature measurements as a function of elevation angle include the total system concept as would be observed during a deep space tracking mission.

B. Collimation Tower

1. Range requirements. One of the DSIF stations, the Venus station (DSS 13),² is equipped with an excellent collimation tower situated approximately 12.7 miles distant near the top of Tiefert Mountain. Figure 10 shows the path profile.³ This path has been found to be essentially multipath free using the 85-ft reflector at S-band (Ref. 2). The X-band performance should be further improved because of the narrower beamwidth of the 85-ft aperture.

A problem associated with the precise evaluation of a large ground antenna using ground-based techniques is that of removing the aperture under test sufficiently far from the exciting source so the phase front across the test aperture may be considered planar. An expression based on uniform illumination of a circular aperture re-

lating the observed gain G , to the true gain at infinity G_0 , is

$$\frac{G}{G_0} = \left(\frac{\sin x}{x} \right)^2 \quad (4)$$

where $G_0 = 4\pi A/\lambda^2$ and $x = \pi D^2/8\lambda R$, where D , λ , and R are the aperture diameter, wavelength, and range, respectively (Ref. 9). A commonly accepted separation, $R = 2D^2/\lambda$, results in an observed gain $G = 0.9872 G_0$. For the Venus station to Tiefert Mountain range, $R = 1.085 D^2/\lambda$ for the 85-ft reflector operated at 8448 MHz. This separation may be considered to lie in the quasi-near-field inasmuch as the phase at the edge of the 85-ft aperture lags the central ray by 41.5 deg and the observed gain $G = 0.9571 G_0$. It is necessary for the system to remain focused at infinity for the observed gain to follow Eq. (4). Because of certain focusing difficulties discussed later, it was decided to peak the antenna gain for the near-field tests by adjusting the hyperboloid. Peak gain occurred with the control room synchro indicator approximately as predicted based on a ray-tracing analysis indicating a near-field best-fit focus would occur with the hyperboloid approximately 0.200 in. toward the apex of the paraboloid compared with the focus position at infinity. Under the above conditions the near-field observed gain will lie within the limits

$$0.9571 G_0 < G < 1.000 G_0$$

or the true gain at infinity, $G_0 = (1.022 \pm 0.022) G$, 3σ .

As an approximate cross-check on the above, two cases were input to the Radiation Pattern Program (Ref. 10), which computes, among other things, axial gain loss as a function of aperture phase illumination. Using the actual (Figs. 7 and 8) rather than uniform amplitude illumination for cases having phase fronts excited from infinity and excited from Tiefert Mountain, a gain of 0.9655 G_0 was obtained when excited from Tiefert Mountain.

The method of ground-based gain measurement planned is considered to be the most reliable among several alternative techniques. Briefly, a known flux is established at the transmitting site and the inverse square law is used to establish the flux at the receiving site. By so doing, serious questions concerning multipath propagation, which often arise when using small comparison apertures at the receiving site, are avoided. The distance between Tiefert Mountain and the 85-ft aperture was accurately measured by tellurometer and found to be 67,320 ft.

²The Venus station is located within the Goldstone complex near Barstow, Calif., in the Mojave Desert.

³Smyth Research Associates of San Diego, Calif., conducted a propagation study of the path and evaluated meteorological and terrain factors (Final Technical Report SRA-603, July 1967).

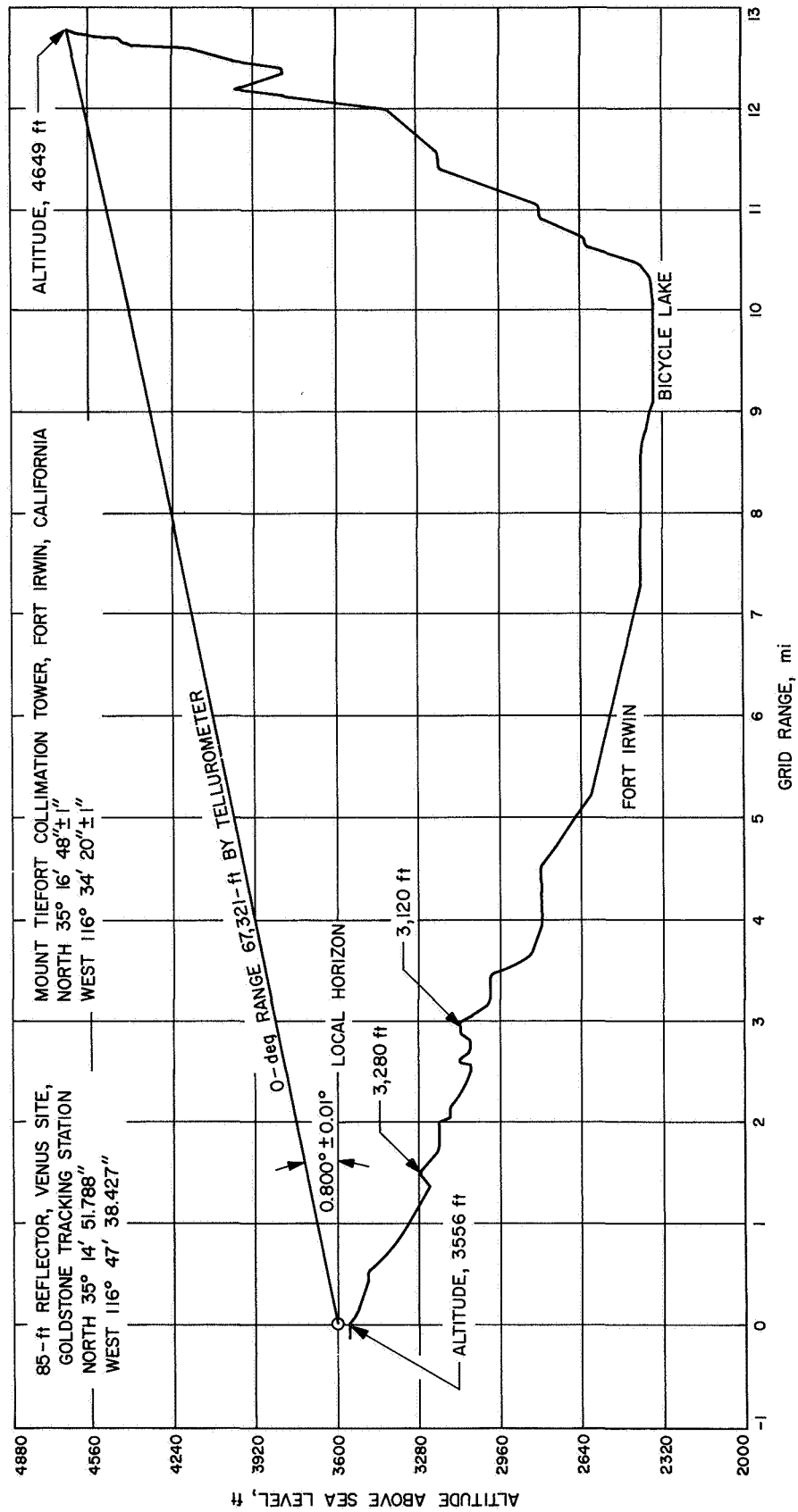


Fig. 10. Path profile, Tiefert Mountain to Venus station

2. Power measurement. In order to establish a known flux, both transmitter power and illuminator antenna gain must be known. Because calibration of an absolute RF power is difficult, a power carefully referenced to a full-scale instrument deflection is obtained at the transmitter site. The same instrument is used at the receiver site and the received power is similarly referenced to the full-scale deflection. By so doing, the absolute reference level need not be known; it was planned to be approximately 10 mW. Figure 11 shows the transmitter equipment used.

The method of gain measurement used requires the accurate determination of the difference between two RF power levels: approximately +30 dBm at the collimation station and approximately -15 dBm at the Venus station. By use of an RF attenuator having precision resettability, but not accuracy, the +30-dBm signal may be calibrated using a standard 10-mW maximum power meter provided the power meter linearity can be established over a 20-dB range (10 mW to -10 dBm). Similarly, the power meter linearity must be established over a 25-dB range (+10 to -15 dBm) to calibrate the received power. The use of a single instrument in this manner precludes any necessity to obtain absolute RF power determinations but does require the accurate determination of linearity over a 25-dB range.

A series of laboratory tests was completed on a Hewlett-Packard Company model 431C power meter (serial 618-00553) when connected to a Hewlett-Packard model H486A (serial 1609) thermistor mount. These tests

were designed and conducted with two major goals: the careful determination of linearity of the power meter and thermistor mount and a determination of drift rates. The method of dc substitution was used, facilitated by use of a Hewlett-Packard model 8402A (serial 243-00124) power meter calibrator. The calibrator simply provides an adjustable constant current source with 100 and $1000 \pm 0.05\%$ Ω sampling resistors in the dc substitute mode. A Hewlett-Packard integrating digital voltmeter (DVM) model 2401B (serial 350-01159) was used as the dc voltage standard. Note that, for a linearity check, thermistor operating resistance need not be determined since operating resistance remains constant (within the ability of the instrument servo loops to reduce the initial disturbance).

The power meter, a new unit, was tested as received. The thermistor mount was modified for improved thermal time constant and isolation.⁴ A foam-filled thin wall stainless steel input waveguide provided isolation; the time constant was improved by adding mass to the thermistor mount. The entire unit was then encased in foam.

A first series of four test runs was made using an auxiliary DVM (Hewlett-Packard model 5265A/5245L) to provide increased resolution over that provided by the meter scale. Table 4 shows a typical run revealing the magnitude of the thermistor thermoelectric effect.

⁴Suggested by C. T. Stelzried of JPL; now commercially available from the Maury Microwave Corporation in the coaxial version. More recently available in WR-90 waveguide from the Hewlett-Packard Company.

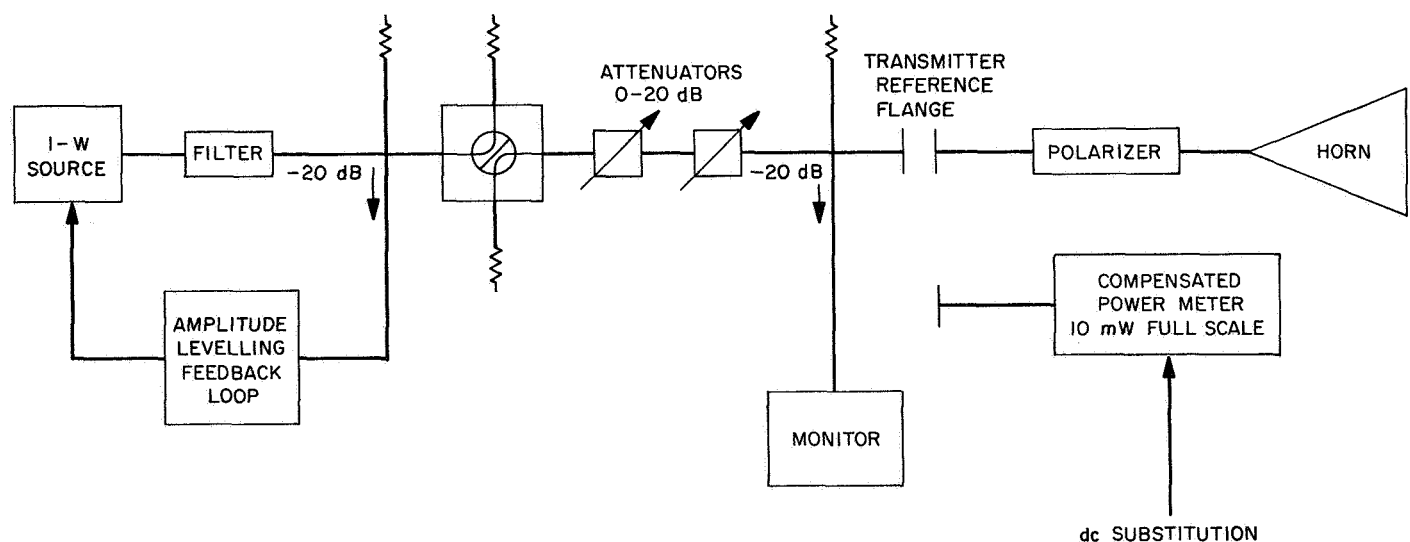


Fig. 11. Tiefert Mountain transmitter equipment

Table 4. Power meter test for thermoelectric effect

Power meter, mW	% scale ^a	Substituted power, mW ^b		Thermoelectric effect, ^c %
		$P_{DC} +$	$P_{DC} -$	
10	100	9.783	9.773	0.10
10	50	4.880	4.873	0.14
3	100	3.075	3.064	0.37
3	50	1.533	1.529	0.27
1	100	0.9810	0.9775	0.36
1	50	0.4893	0.4869	0.49
0.3	100	0.3108	0.3089	0.61
0.3	50	0.1550	0.1539	0.71
0.1	100	0.1034	0.1024	1.00
0.1	50	0.05170	0.05098	1.38
0.03	100	0.03114	0.03064	1.62
0.03	50	0.01560	0.01525	1.62
0.01	100	0.009923	0.009610	3.2
0.01	50	0.004973	0.004774	4.0

^a100% and 50% scale is defined as being produced on the auxiliary digital voltmeter, following zero set, with no correction for input impedance of 10 MΩ.

^bSubstituted power = $[V_c / (2 \times 10^3)]^2 R_T$ for the 10 and 3 mW scales (100-Ω sample).

Substituted power = $[V_c / (2 \times 10^3)]^2 R_T$ for all other scales (1000-Ω sample), where V_c is the impedance-corrected dc voltage across the sampling resistor, and R_T is the nominal thermistor operating resistance, set equal to 100Ω, all data.

^cThermoelectric effect is defined as $(P_{DC+} - P_{DC-}) / P_{DC+}$

A single second test was performed using the 2401B DVM to provide both the increased meter scale resolution and the voltage standard functions. A single test was felt to provide data more typical of those experienced under field conditions. Table 5 shows the averaged first series compared with the single second test. It is interesting to note that the error of the single test is generally less than 0.1% compared with the smoothed data, with the exception of the 3-mW scale. The 3-mW scale was later found to be excessively noisy.

The smoothed and single run data were each normalized to the full-scale value and converted to dB. Table 6 shows the deviations for each scale, in dB, from 100% to 50% scale (0.000 to -3.010, -5.000 to -8.010 dB, etc.). Apparent factory alignment errors of 1% and 5% in the 3- and 0.1-mW scale data were adjusted in Table 6 to gain a better view of the attainable linearity. The linearity (100% to 50% of scale) is (0.013 ± 0.002) dB standard deviation. The linearity from 100% to 100% of next

Table 5. Power meter test: smoothed and single test comparison

Power meter, mW	% scale ^a	Substituted power, mW ^b (mean of 4 runs in first series)	Substituted power, mW ^b (single second test)	Error of the single test, ^c %
10	100	9.784	9.782	-0.02
10	50	4.878	4.880	+0.04
3	100	3.068	3.060	-0.27
3	50	1.529	1.525	-0.26
1	100	0.9799	0.9800	+0.10
1	50	0.4882	0.4883	+0.02
0.3	100	0.3099	0.3101	+0.07
0.3	50	0.1544	0.1545	+0.07
0.1	100	0.1030	0.1029	-0.10
0.1	50	0.05135	0.05132	-0.06
0.03	100	0.03094	0.03094	0.00
0.03	50	0.01544	0.01543	-0.07
0.01	100	0.009786	0.009785	-0.01
0.01	50	0.004879	0.004876	-0.06

^aAs before, 100% and 50% scale is defined as being produced on the auxiliary digital voltmeter, following zero set, with no correction for input impedance. Input impedance is 10 MΩ for 4 runs, 1 MΩ for second test.

^bCorrected for thermoelectric effect.

^cError is defined as (single test - mean of 4 runs)/mean.

scale (0.000 to -5.000, -5.000 to -10.000 dB, etc.) is approximately 0.0035 ± 0.0035 dB standard deviation.

The 50% scale data show a definite error on each scale of -0.3%, attributable to the squaring circuit.⁵ The 100% to 100% scale data show about four times better performance, on the verge of being resolution-limited,

⁵Discussions with Jim Macrie and Fred Praman of Hewlett-Packard, Palo Alto, Calif., showed that the squaring circuit was originally designed for $\pm 0.25\%$ linearity. The error due to finite loop gain not allowing a complete rebalancing of thermistor operating resistance is estimated to be 1/10 or less of the squaring circuit error. The thermoelectric effect exhibited by serial 1609 thermistor is about twice the average. Also, comments are of interest concerning effective efficiency, i.e., the dc-RF conversion factor. For the single detection element (waveguide) type mounts there is no known reason for suspecting efficiency to change with applied power levels. In the case of the dual detection element (coaxial) mounts, either balanced or unbalanced, there is a known dual element error, apparent when operating on the upper ranges of the instrument when the applied RF power causes a decrease in bias power of nearly equal magnitude. This error is controlled, at manufacture, to something better than 0.1%.

Table 6. Power meter test for linearity

Power meter, mW	% scale	Deviation, dB ^a (first series)	Deviation, dB ^a (single second test)	Single scale 3-dB linearity, dB (first series)	Single scale 3-dB linearity, dB (single second test)
10	100	0.000 ^b	0.000 ^b		
10	50	-0.013	-0.011	-0.013	-0.011
3°	100	+0.013	0.000		
3°	50	-0.001	-0.011	-0.014	-0.011
1	100	+0.006	+0.008		
1	50	-0.009	-0.007	-0.015	-0.015
0.3	100	+0.007	+0.011		
0.3	50	-0.009	-0.005	-0.016	-0.016
0.1 ^d	100	+0.003	+0.002		
0.1 ^d	50	-0.009	-0.012	-0.012	-0.014
0.03	100	0.000	+0.001		
0.03	50	-0.009	-0.011	-0.009	-0.012
0.01	100	+0.001	+0.001		
0.01	50	-0.011	-0.014	-0.012	-0.015

^aDeviation is here defined as measured-indicated.

^bApproximately 0.02% error in data adjustment of each full scale to 0.000 dB. See Table 5.

^cAdjusted data +0.050 dB (1%); apparent factory error. (The instrument requires alignment of potentiometer A2R6, full scale accuracy adjustment in the dc feedback current generator.)

^dAdjusted data -0.220 dB (5%); apparent factory error. (The instrument also requires alignment of potentiometer A2R3, same circuit.)

Table 7. Power meter test for drift

Power meter, mW	Power meter output, mV dc			Full scale uncertainty, %
	0 set	50% scale	100% scale	
10	±0.03	±0.10	±0.10	0.01
3	0.03	0.10	0.10	0.01
1	0.05	0.10	0.10	0.01
0.3	0.10	0.10	0.10	0.01
0.1	0.20	0.20	0.20	0.02
0.03	0.50	0.50	0.50	0.05
0.01	1.0	1.0	1.0	0.10

The instrument, when carefully used with a thermally improved thermistor head, is seen to be limited by the squaring circuit to 0.3%. With reasonable field instrumentation, dc substitution can be very conveniently applied for an accuracy of 0.1% or better over a 30-dB range. The worst-case short-term drift (~1 min) experienced during the laboratory tests represents a thermal change of 10^{-4} °C, due to thermistor and bridge constants producing a sensitivity of about $100 \mu\text{W}/^\circ\text{C}$. In summary, it was felt the determination of reasonably high (-15 dBm or greater) power levels for the ground-based tests presented no serious problem.

3. Gain standard horn measurement. Calibrations of gain standard horns is a problem of continuing interest at JPL and elsewhere since the errors involved are the largest unknown in this type of test. The nominal 22-dB gain (4.671λ) aperture dual mode horn used as the primary feed (Figs. 3-5) has been carefully studied by Ludwig (Ref. 11). This horn is somewhat broadbeamed, however, for the Tiefert Mountain range shown in Fig. 10. Also, the received power at the 85-ft antenna would be less than the -15 dBm level preferred. For this reason primarily, and for possible further reduction of multipath, the development of a large aperture (12.548λ) gain standard horn was initiated. Figures 12-14 show the 8448-MHz E-, H-, and 45-deg-plane patterns of the finished device. Figure 15 shows the horn undergoing precision radiation pattern tests. The technique described by Ludwig (Ref. 11) was carefully applied; the resultant directivity was found to be +29.520 dB when integrating angular expanded patterns to the -40-dB level and assuming the remainder to be zero. When integrating to the -80-dB level, the directivity decreased as expected. The final value was +29.510 dB. Estimated

with the exception of the two scales requiring alignment. It will be noted in both the thermoelectric effect data and the Table 5 data that the 3-mW scale was consistently noisy.

Data related to the drift problem were taken by observing the ability to establish and hold the zero, 50% and 100% scale deflections using the adjustable calibrator source. Table 7 summarizes the drifts experienced during a single substitution (~1 min). Table 7 data represent four attempts at each level on each scale.

All tests utilized the 2401B voltmeter at 1-s integration; the power meter calibration factor was constant at 98%. As the results show, full-scale deflection occurs with dc substituted power within 0.17% of the theoretical value on the highest range.

turnstile junction and horn losses are 0.025 and 0.023 dB, respectively. Based primarily on a foundation of experience with the +22-dB horn and a few pessimistic assumptions, a tolerance of ± 0.45 dB (3σ) has been assigned to the large aperture horn gain. Figure 16 shows the horn installed at Tiefort Mountain, optically bore-

sighted, and arranged to position all electronic equipment within the personnel shelter. An uncalibrated +22-dB horn fitted with a rotating joint was also used, for measurement of the ellipticity of the 85-ft antenna. The lower flux obtained caused this measurement to be done using the crystal mixer radiometer.

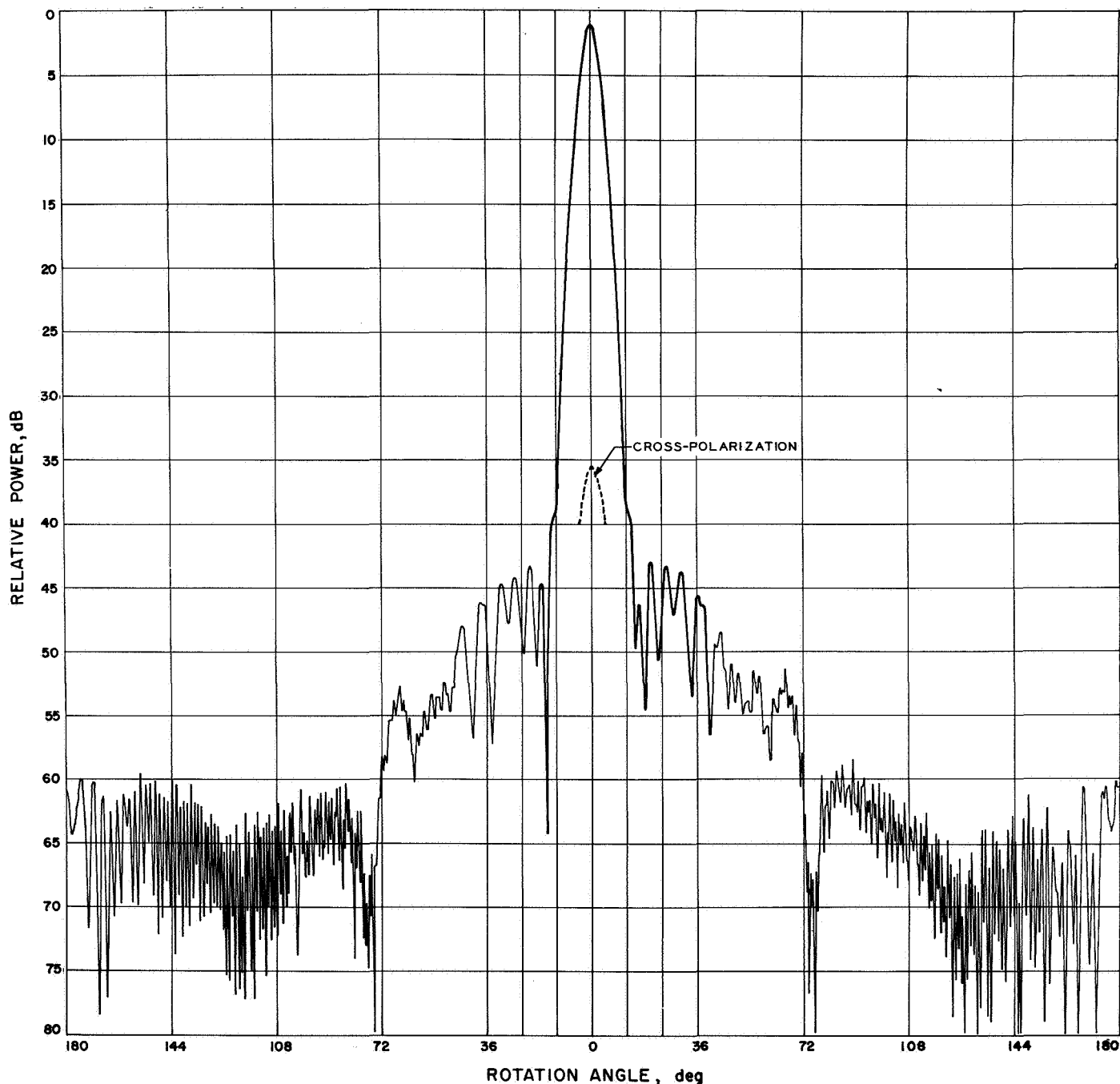


Fig. 12. Radiation pattern, large aperture gain standard horn, E-plane

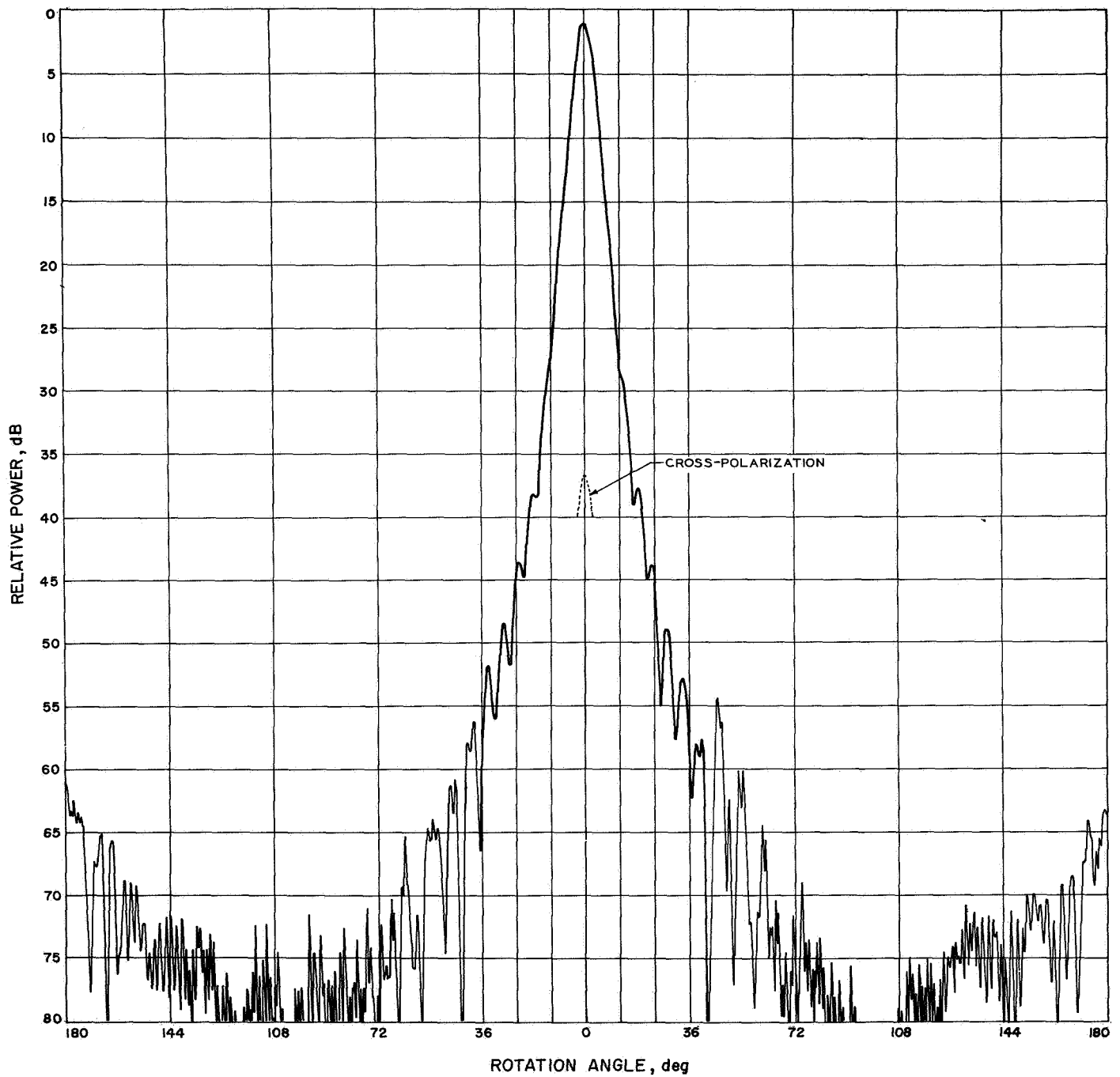


Fig. 13. Radiation pattern, large aperture gain standard horn, H-plane

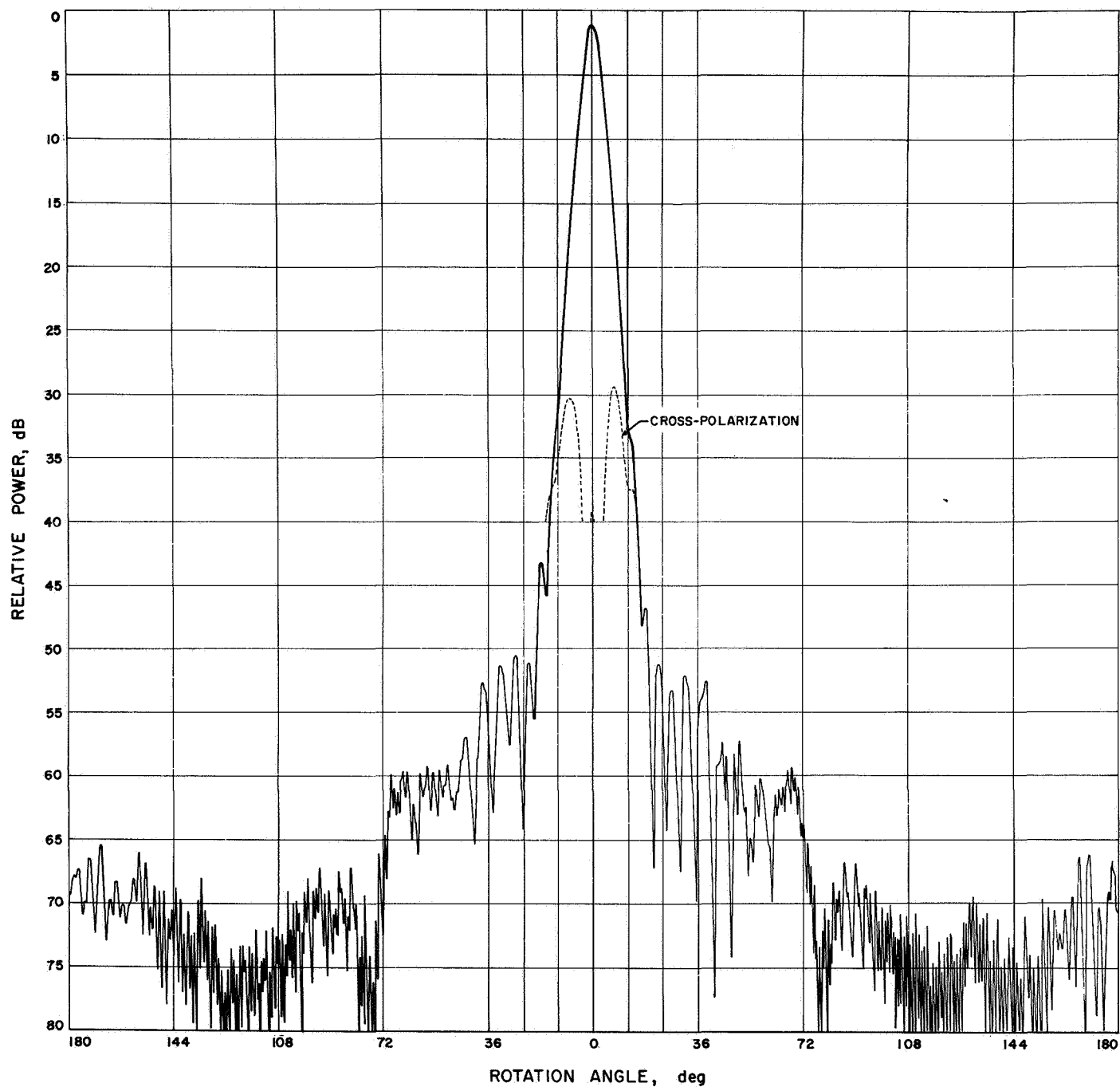
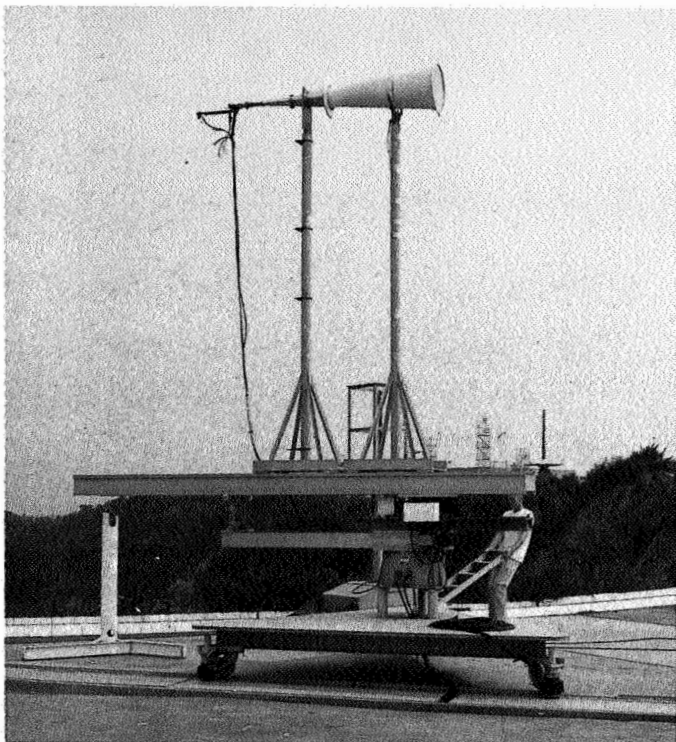
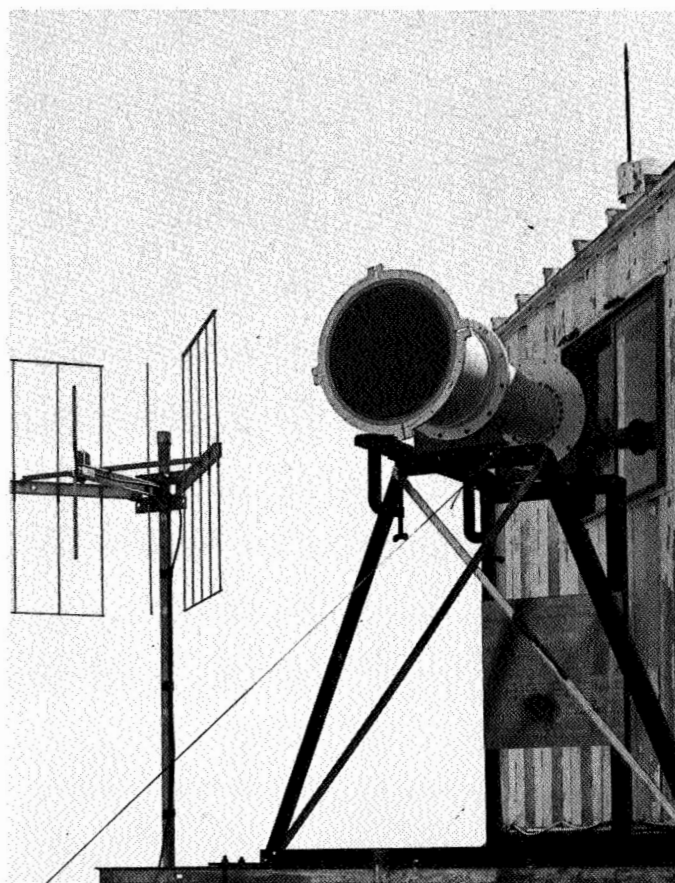


Fig. 14. Radiation pattern, large aperture gain standard horn, 45-deg-plane



**Fig. 15. Large aperture gain standard horn
pattern test range**



**Fig. 16. Large aperture gain standard horn
at Tiefort Mountain**

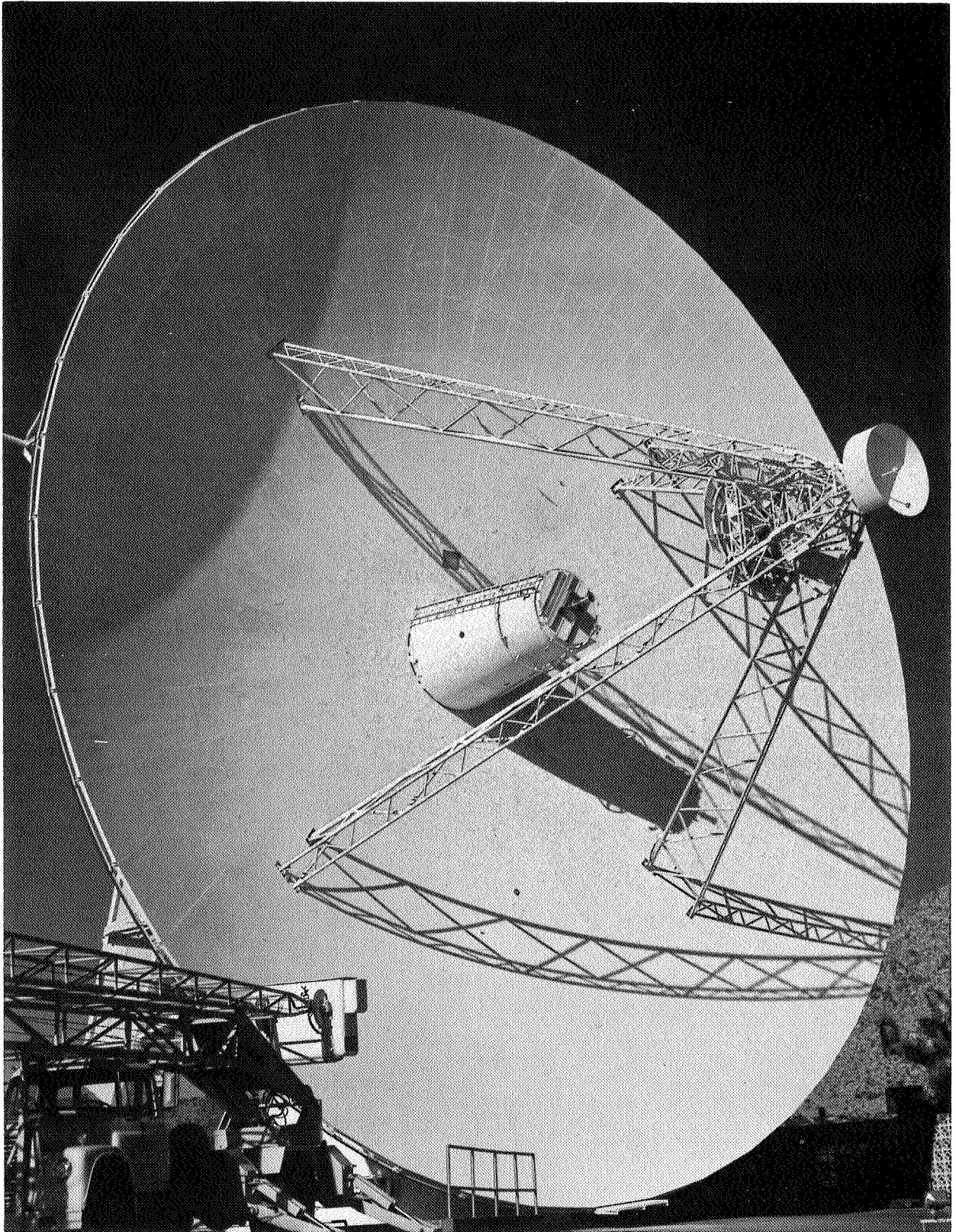


Fig. 17. XCE feedcone installed on Venus station az-el reflector

IV. Initial Measurements, November 1966

The XCE feedcone was installed on the Venus 85-ft az-el reflector early in November 1966 (Fig. 17). Considerable difficulty was immediately found in determining a hyperboloid setting to optimize antenna gain. Results were not repeatable on a day-to-day basis, and peak-to-peak RF pointing repeatability was occasionally as bad as ± 0.050 deg. One effect causing even further confusion was the fact that, once an approximate focus position was obtained on Cygnus, at approximately 60 deg elevation angle, it was decided to cross-check the collimation tower focus setting, which had been predicted on the basis of ray optics to occur with the hyperboloid approximately 0.200 in. toward the *apex* of the paraboloid, compared with the far-field focus position. The tests indicated essentially the opposite was required; i.e., the hyperboloid had to be positioned 0.280 in. toward the *vertex* of the paraboloid to approximately focus the system on Tiefert Mountain. Under these uncertain conditions a careful collimation tower gain test using the precision ground-based techniques developed appeared a waste of valuable test time. The +22-dB horn at Tiefert Mountain, configured for rotating linear polarization, was used to verify the ellipticity of the 85-ft system, which was less than 0.45 dB. No further collimation tower work was attempted during this period. The 85-ft system was roughly refocused on Cygnus at 60 deg elevation angle, and source temperature measurements, defined at the maser reference flange, were made.

The results of the Cygnus tracking during this period gave an excess system temperature defined at the maser reference flange of $(15.5 \pm 2.3)^\circ\text{K}$, 3σ , for the source between 40 and 75 deg elevation. Ignoring possible small bias errors and considering only the random errors in measurement scatter and flux uncertainty, the initial efficiency was $(45.6 \pm 9.9)\%$, 3σ , or a gain of $(+63.80 \pm 0.96)$ dB, 3σ , both defined at the maser reference flange and applicable over a restricted elevation angle range. By assignment of the remaining loss, after subtracting out the overall feed system, dissipation, and blockage losses, to the surface tolerance, a mean value of 0.063 in. rms was obtained.

V. Supporting Studies

Following the initial X-band tests at the Venus station, a review of the existing body of knowledge concerning the structural characteristics of the antenna was performed. Extensometer tests nearly 2 yr previous to the

X-band tests had shown mechanical hysteresis effects due to looseness in the bolted joints comprising the backup structure. Although the antenna had been continuously operated at S-band for over 5 yr, the loose nature of the structure had not been observed at the longer wavelength.

Since the antenna pointing system, as read out using the available Datex indicators, was known to be in fair condition, the poor pointing and nonrepeatable focusing was ascribed to the tipping part of the structure, i.e., that portion decoupled from the indicators. Theodolite measurements of approximately 600 targets on the reflector panels were made during March 1967. These tests were conducted under two conditions: the first with the reflector at a rest position for a few days and the second with the reflector exercised, brought to a rest position, and measured in a rather brief period (brief compared with some techniques) of approximately 4 h. A program of structural rebolting was initiated following these tests. By early June 1967, the reflector box girder had been completely rebolted and a second series of theodolite measurements were made using the same procedures adopted earlier.

The field data was input to the JPL Best Fit Paraboloid Program (Ref. 12). This program gives the root mean square of $1/2$ the RF pathlength of the residuals following best-fitting to a perfect paraboloid. The perfect paraboloid is free to assume a new focal length as one of the fitting parameters. Table 8 summarizes the reduced field data. The rms of $1/2$ the RF pathlengths is seen to vary 0.035–0.045 in. This value is representative of the approximately 600 observed targets essentially firmly attached to the backup structure; an overall surface tolerance figure must also take into account surface panel and hyperboloid manufacturing and setting errors.

No significant difference between data sets in Table 8 is seen. It is concluded most of the structural looseness occurs in the rib trusses and hoops which were not yet rebolted. The focal length from zenith to horizon attitudes is seen to change 0.40–0.50 in. Movement of the entire quadripod structure relative to the best-fit focal length may effectively change these computed values as observed in RF tests. The mechanical hysteresis shows up in both the rms and focal length values as suspected.

At this point, the X-band RF test results began to appear reasonable. The focusing, which was confusing

Table 8. Field data: 85-ft az-el surface tolerance^a

Date, 1967	rms case	Reflector attitude	rms, in.	Focal length, in.	Comments	Wind, mph
2/28	8	Zenith	0.039	432.06	Structure at rest 7 days	0
3/1	4	Zenith	0.044	432.03	Structure exercised at 45 deg elevation	0
3/6	6	45 deg	0.042	431.79	Moved zenith to 45 deg elevation	10-25
3/7	5	45 deg	0.039	431.84	Moved zenith to horizon to 45 deg elevation	—
3/8	3	Horizon	0.036	431.68	Moved zenith to horizon	—
3/27	10	Zenith	0.045	432.05	Structure at rest 2 days	—
6/2	7	Zenith	0.041	432.21	Structure at rest 2 days	20-38
6/2	1	Zenith	0.039	432.10	Structure exercised at 45 deg elevation	20
6/3	2	45 deg	0.035	431.87	Structure at rest 2 h	20-35
6/6	9	Zenith	0.040	432.11	Structure at rest 20 h	—

^aBased on 570-590 points in analysis, no area weighting, and focal length fit for rms.

during the initial tests, could be explained as follows: Once focused on Cygnus A at a relatively high elevation angle, the antenna was then oriented to the horizon for collimation tower observation. The focal length decreased roughly 0.50 in. In order to focus at infinity at the horizon, it would be required to move the hyperboloid toward the vertex of the paraboloid this amount. Then, to account for the near-field nature of the collimation tower, a movement back toward the apex of about 0.20 in., as predicted, would be required, leaving a net movement of the hyperboloid of approximately 0.30 in. toward the vertex of the paraboloid. As discussed above, the experimentally obtained value was 0.28 in. in this direction.

Because the STAIR structural computing program (Ref. 13), together with the JPL Best Fit Paraboloid Program, had been extensively utilized to analyze and design the NASA/JPL 210-ft Advanced Antenna System, this program pair was applied to the 85-ft az-el.⁶ Although field tests on the 210-ft structure agree well with computed results, this is not the case with the 85-ft structure. There are additive deflections in the actual 85-ft structure over the computed results caused by compromises made to ease fabrication. The optimum condition of the centroids of all structural members joining at the work points is missed by a few inches on the 85-ft structure, but assumed optimum, as required by the STAIR program, in the analysis. Therefore bending, as well as axial,

forces are generated in various members, resulting in additional deflections.

Tables 9 and 10 give the fitted focal length and rms values as computed using the STAIR and Best Fit programs for the idealized 85-ft structure. In order to account for the idealization made, cases with 2 and 3 times

Table 9. Computed data: 85-ft az-el best fit focal lengths

Reflector attitude	Focal length 1 × symmetrical deflections, in.	Focal length 2 × symmetrical deflections, in.	Focal length 3 × symmetrical deflections, in.
Zenith	432.194	—	—
45 deg	432.000	432.000	432.000
Horizon	431.709	431.453	431.199

Table 10. Computed data: 85-ft az-el rms of one-half RF pathlengths

Reflector attitude	rms 1 × symmetrical deflections, in.	rms 2 × symmetrical deflections, in.	rms 3 × symmetrical deflections, in.
Zenith	0.018	—	—
45 deg	0	0	0
Horizon	0.026	0.050	0.074

⁶Private communication, M. S. Katow. (See also Ref. 14.)

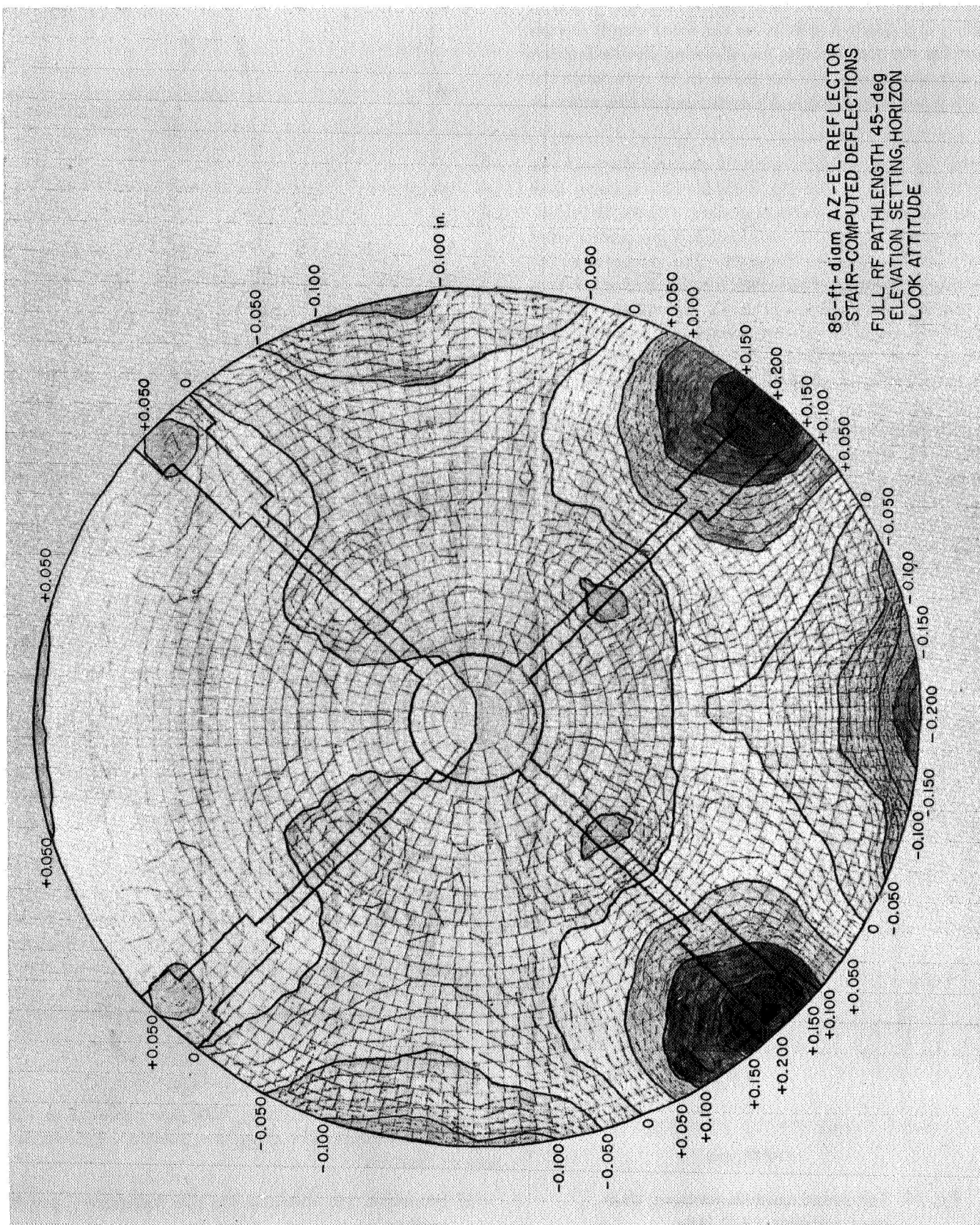


Fig. 18. Computed surface contour map, 85-ft az-el reflector

the deflections were generated. Apparently the idealized model used properly accounts for the focal length change but not for the rms change. In all cases, the deflections at 45 deg elevation angle are taken to be zero since the reflector panels were originally optimized in this attitude.

Figure 18 is a machine-plotted contour map of the best-fitted STAIR computed data for the horizon look attitude, using the 1× deflection data. Figure 18 is calibrated in terms of full RF pathlength, a parameter used in the Radiation Pattern Program. The purpose of the figure was to arrange input data for the Radiation Program digitized in sufficiently small increments to form subapertures capable of reasonably representing the quadripod and subreflector blocking. Approximately 2500 near-equal-area subapertures were formed. Feed amplitude and phase data shown in Figs. 7 and 8 were used, with the phase data suitably altered to account for the near-field collimation tower, as input to the program. Figures 19 and 20 show computed azimuth and elevation plane patterns of the system, as would be observed using Tiefert Mountain, for the 1× and 3× deflection data. It was expected that measured radiation patterns should reasonably agree within these limits.

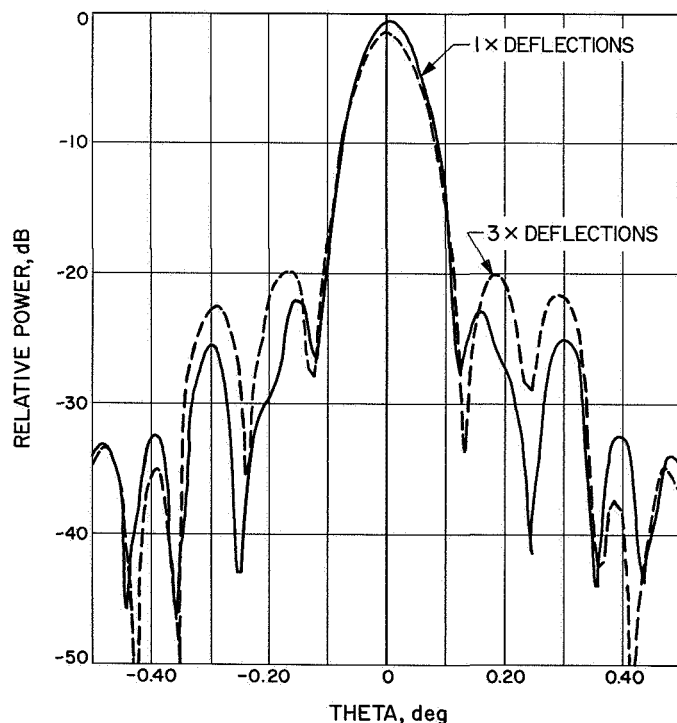


Fig. 19. Computed azimuth patterns, 85-ft az-el reflector, 8448 MHz

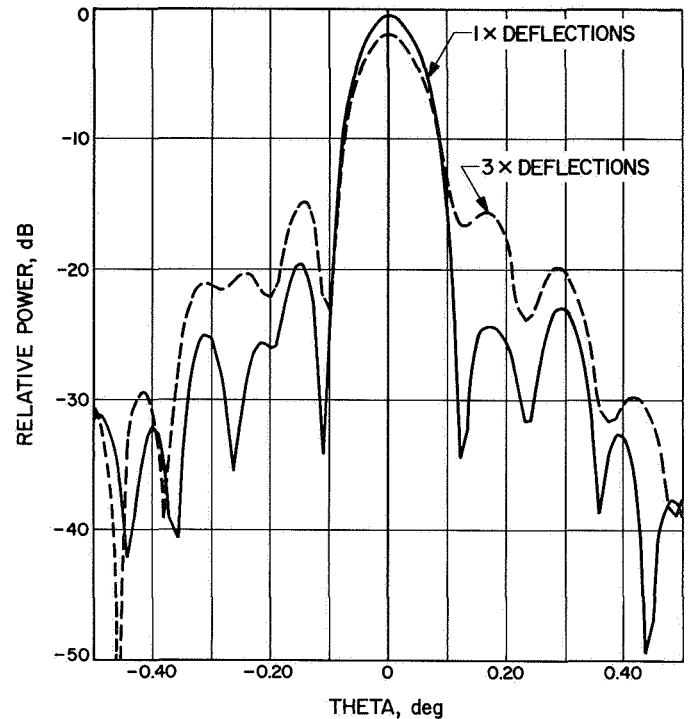


Fig. 20. Computed elevation patterns, 85-ft az-el reflector, 8448 MHz

VI. Final Measurements, June 1967

A. Radio Astronomical

Following the box girder rebolting, a 2-wk opportunity to operate the 85-ft antenna at X-band became available. Armed with the initial measurements and the supporting studies, it was felt a reasonable background had been obtained to plan an efficient test series.

During the June 1967 tests, the initial effort was to focus the system as a function of elevation angle, since the earlier data proved focal length changes of about 0.5 in. were present. The loss of gain due to defocusing by this amount is a maximum of 12% at X-band; thus, proper focusing is a very important consideration, particularly for the calibration and evaluation work being performed.

On the nights of June 14-15, 1967, Cygnus A was tracked in the usual manner, with one addition to the standard procedure. The complete procedure for one run was as follows:

- (1) Boresight the antenna by the half-power points method.

- (2) Obtain the usual five on-source Y-factor measurements.
- (3) Run the hyperboloid in and out in the axial direction through a reasonable range, while open-loop-recording the radiometer output, and noting the elevation angle of the source. Return to the focus setting used in step (1).
- (4) Obtain the usual five off-source Y-factor measurements.
- (5) Repeat steps 2, 3, and 4 four additional times.

The purpose of step 3 is to obtain a focus curve for that particular elevation angle. A total of 91 curves were obtained, beginning on the first night at about 65 deg elevation, rising to 85 deg and setting. On the next night, a complete track was obtained. The focus curves were reduced to obtain the maximum gain setting of the hyperboloid, in inches from an arbitrary reference, as a function of elevation angle.

Figure 21 shows 90 data points obtained as previously described. The curves were drawn to assist in interpretation of the data; no sophisticated attempt was made to best-fit the data. As can be seen, however, the bulk of the data fits well. Because the physical placement of the feedhorn in a cassegrain-fed antenna is relatively non-critical when compared with the physical placement of the hyperboloid (both with respect to the best-fit paraboloid), the change in hyperboloid setting required for maximum gain is directly the change in focal length of the best-fit paraboloid.⁷ Thus, as shown in Fig. 21, the total focal length change as seen by RF is about 0.6 in. Also, the June 14 data were not repeated on June 15. On both days, about 0.2 in. total hysteresis is indicated, and reaches a maximum at about 45 deg elevation. The hysteresis is further indicated by the characteristic plateau of the longest focal lengths occurring, not at the near-zenith position, but somewhat later in time during the

⁷This statement ignores possible movement of the entire quadripod structure with respect to the best-fit paraboloid vertex.

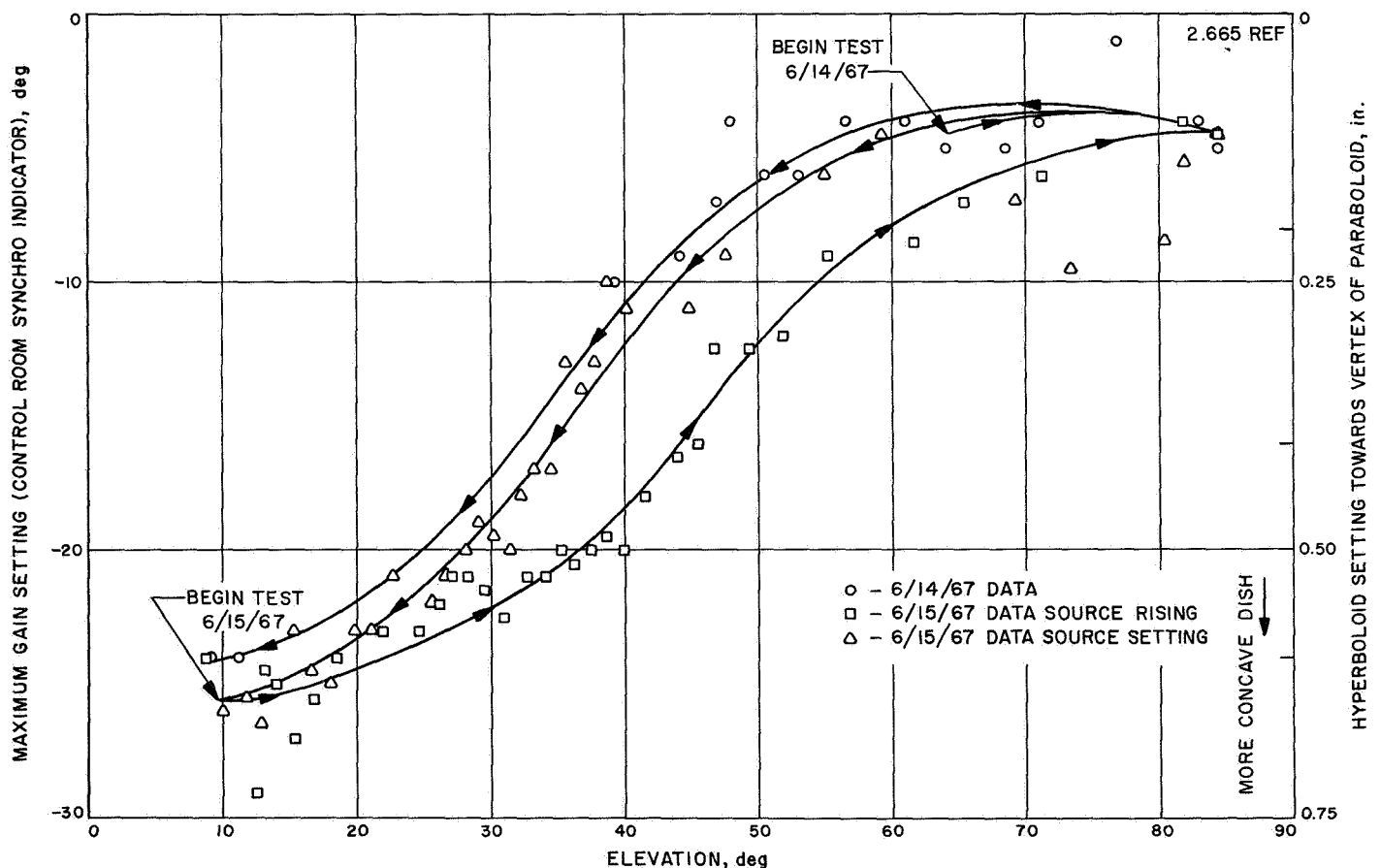


Fig. 21. Cygnus A focusing as a function of elevation angle, 85-ft az-el reflector, X-band

tracking after the source has decreased to about 70 deg elevation. This occurrence might be explained as a time lag for the paraboloid structure to slowly settle into a more shallow dish when near zenith, and the reversal of the elevation drives and downward motion does not immediately cause a structural trend toward the deeper dish seen at low elevation angles. Focus curves obtained at low elevation angles were distinctly broader than the fairly sharp focusing obtainable at higher angles. A selected fixed focus of -5 deg in Fig. 21 was made to optimize the high angle (~ 75 deg elevation) source temperature measurements.

Data were also collected to examine beam pointing stability. Figure 22 represents about 160 required elevation axis angle offsets as a function of elevation angle. These data were collected from June 8 to 10, 1967. Figure 22 may be thought of, primarily, as a smooth curve that is the sum of several mechanically induced deflections, but usually dominant is the rotation and translation of the best-fit paraboloid. The pointing is then interpreted to have a 3σ jitter for this axis of about ± 0.020 deg.

Figure 23 shows about 370 measured excess system temperatures referenced to the maser input flange for Cygnus A during June 1967, with the antenna fix-focused as discussed above. Each measurement is the mean of differencing five determinations of ambient load to antenna Y-factor on-source with five determinations of ambient load to antenna Y-factor off-source. The RF beam was boresighted on-source at approximately 30–60 min intervals with updated ephemeris tape drive controlling pointing between boresights. Off-source system temperature measurements are made by alternately slewing ± 2.0 deg from the source in elevation when the source is above 45 deg and ± 2.0 deg in azimuth when the source is below 45 deg elevation. Only 2–3% of the total June 1967 data was rejected as blunder points.

Figure 23 includes a third-order polynomial curve which was fit to the data without weighting. Also, a sample interval of 10 deg elevation angle was selected. The center of each vertical bar in Fig. 23 represents the sample mean excess system temperature (at the sample mean elevation angle) in that 10-deg elevation angle increment. The bars represent the square root of the sample variance, which is essentially one standard deviation about the sample mean except for the lowest elevation increment. A fourth-order polynomial curve was fit to the data with each point weighted inversely to the

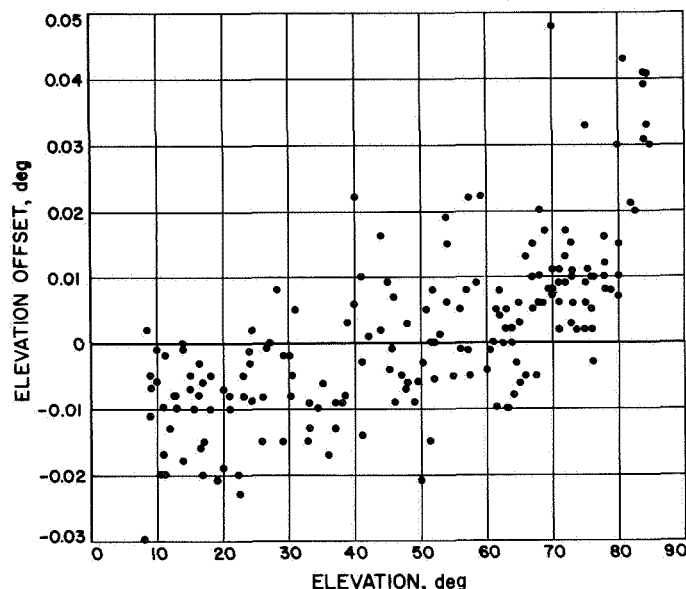


Fig. 22. Elevation offsets as a function of elevation angle, 85-ft az-el reflector, X-band, June 1967

probable error. The probable error was taken as the root sum square of the probable errors of the individual on-source and off-source temperature measurements. No significant difference exists between that curve and Fig. 23. Indeed, the apparently anomalous low temperatures observed between 10 and 35 deg elevation were individually examined; the probable errors of the on-source and off-source temperatures for those data are not unlike any of the data and therefore appear to be real. It was expected that poor pointing or radiometer gain changes would be indicated by increased jitter among the individual determinations. Possibly significant is the fact that data between 40 and 60 deg elevation exhibits the smallest jitter.

The peak temperature observed at 60 deg elevation is thought due to (1) the paraboloid surface, which was adjusted to be optimum at 45 deg elevation, and (2) the focus setting, which was adjusted to be optimum at 75 deg elevation as discussed. Because atmospheric extinction is expected to be a very small effect at these elevation angles, it is reasonable to expect the highest temperatures to be observed between 45 and 75 deg elevation.

The weighted mean of the June 1967 data between 40 and 70 deg elevation is $(15.7 \pm 3.0)^{\circ}\text{K}$, 3σ , which is nearly identical to the November 1966 result of $(15.5 \pm 2.3)^{\circ}\text{K}$, 3σ . The increased temperature is thought due to better focusing, while the increased jitter is most

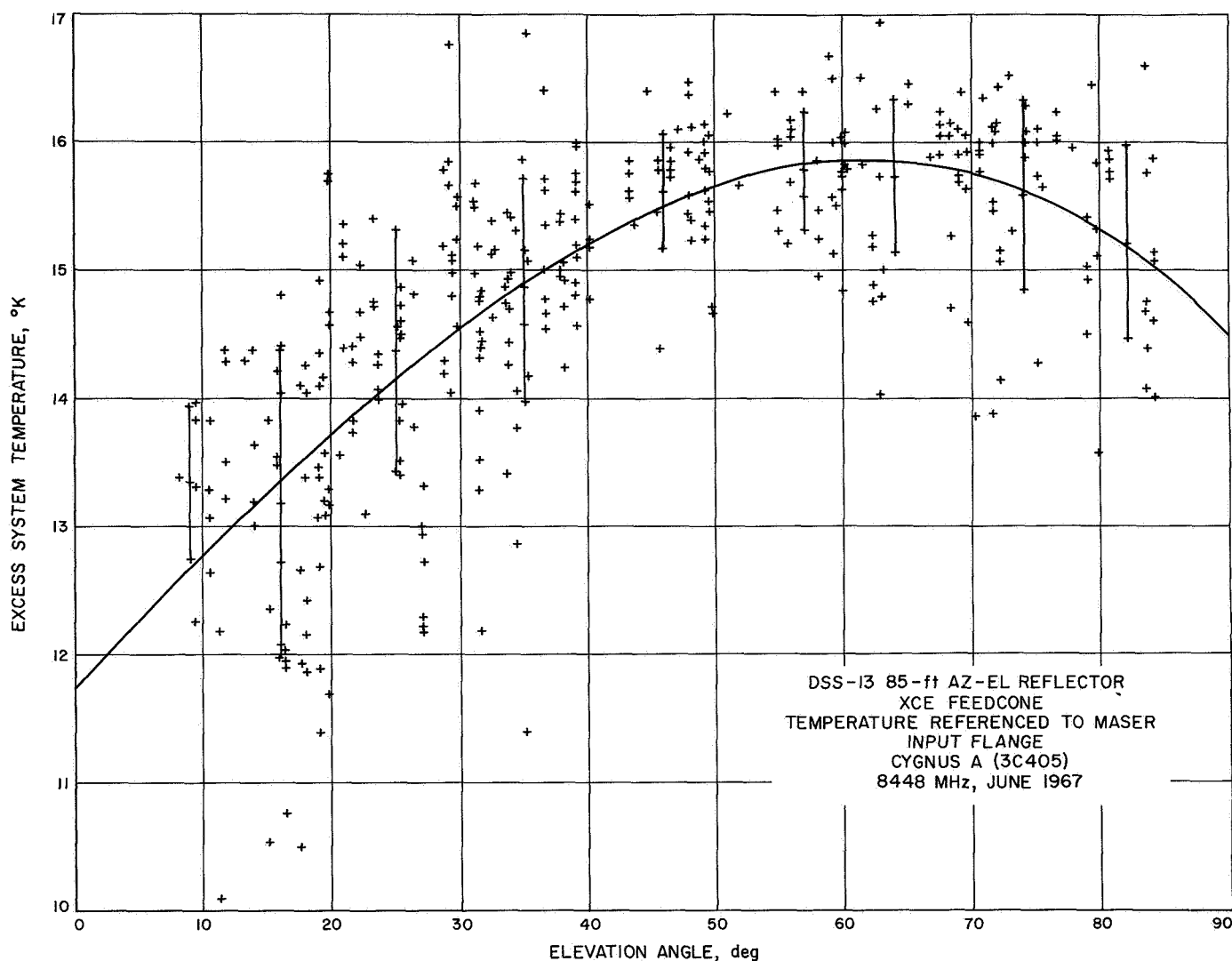


Fig. 23. Excess system temperature referenced to maser input flange, Cygnus A

probably a result of more extensive sampling. A final value for the efficiency, defined at the maser input flange and applicable over 40–70 deg elevation is $(46.2 \pm 11.2)\%$, 3σ , where the tolerance is taken as the root sum square of the standard deviations of the selected flux density for Cygnus A and the measurement scatter. For the data reported here, the measurement scatter exceeds the flux density uncertainty. As a scale factor for the convenience of the reader, the mean system efficiency during June 1967 is greater than 40% (13.6°K excess system temperature in Fig. 23) for elevation angles greater than 20 deg.

Data presented in the form of Fig. 23 are useful for a deep space communications system designer, as discussed earlier. Of interest to the antenna designer and/or

radio astronomer is to separate the various loss contributions. Only the defocusing effect due to paraboloid focal length change has been evaluated. Based on focus data shown before, nearly 0.4λ axial misalignment of the cassegrain subreflector at 10 deg elevation angle occurs. This axial misalignment, if corrected, would increase the observed excess system temperatures approximately 1.9°K at 10 deg elevation. Although not carefully evaluated, atmospheric extinction appears less than half the defocusing loss.

Figure 24 shows the corresponding cold sky measurements, taken in conjunction with Fig. 23 data. Because all data were simply plotted without regard to day number or weather, it was first suspected the large spread among data at low elevation angles was due to weather.

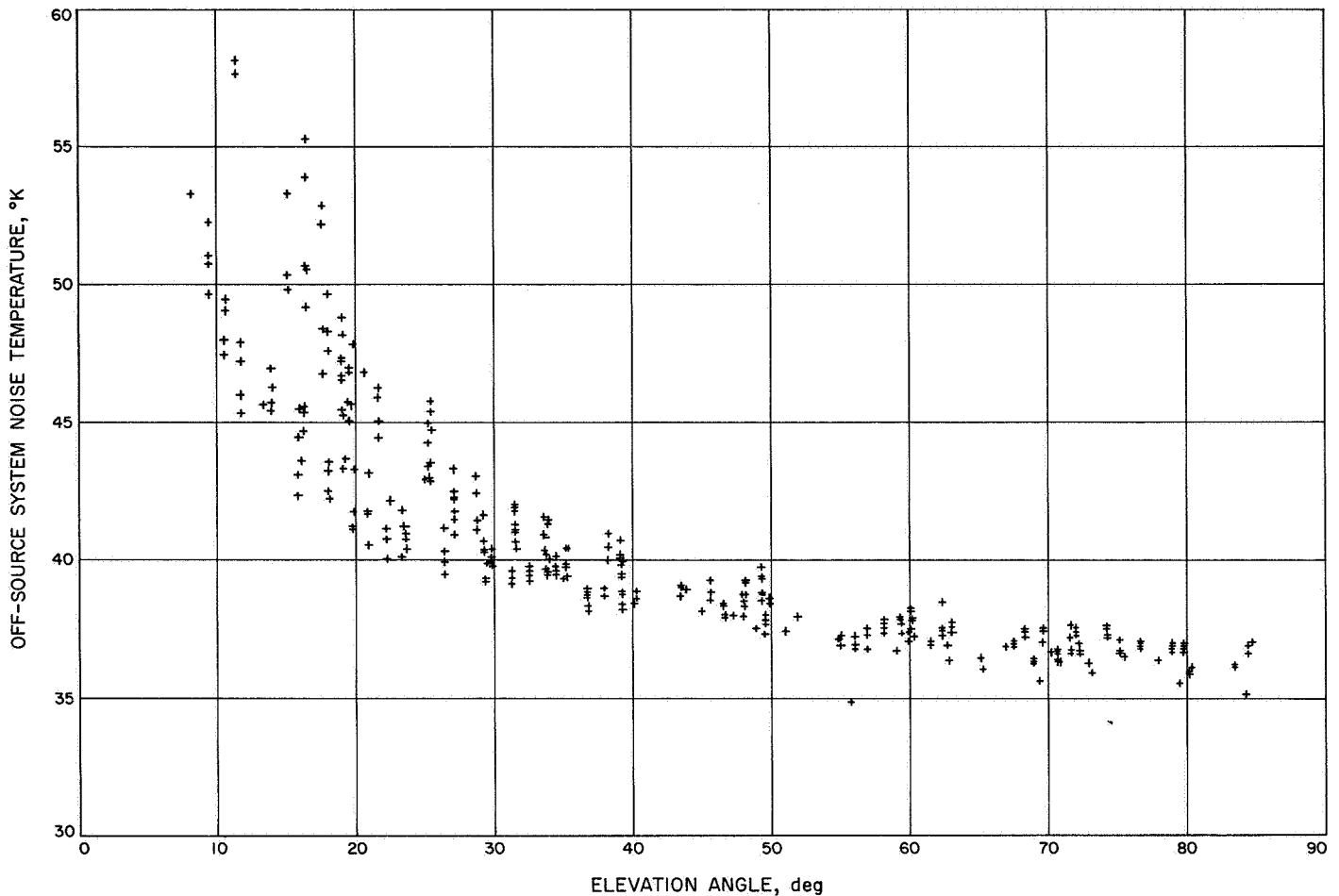


Fig. 24. Off-source system temperature referenced to maser input flange

Closer examination of the raw data proved nearly all low temperatures below 40 deg elevation occurred when looking approximately 90 deg azimuth, or east, and nearly all high temperatures occurred observing toward the west. The land mask at the Venus station is generally below 0.5 deg elevation looking east but is always above 3 deg and as high as 13 deg between azimuths of 200 and 360 deg. It is clear the high measured temperature portion of Fig. 24 is due to the land mask at the Venus station.

Of further interest in Fig. 24 is the increase in system noise from zenith to 10 deg elevation, which, for the favorable land mask direction, is only 13–14°K. This value is indicative of the high dry siting of the Goldstone complex; a comparable value at S-band using the archetype feed is 11°K (Ref. 2). Because antenna sidelobe, spillover, and blockage effects are of second-order importance, the increase in system noise temperature is nearly totally related to the main beam observing atmospheric noise.

Table 11 gives the average off-source temperatures and standard deviations of the data. Average temperatures and standard deviations below 30 deg elevation are qualified as including both sets of data (source rising and setting).

B. Ground Based

On June 21, 1967, the Tiefert Mountain station was configured with the previously described +29.510-dB gain standard horn excited with right-hand circular polarization (RCP) by the turnstile junction polarizer. The laboratory-calibrated portable thermistor power bridge previously discussed was rechecked in the field for linearity using dc substitution to an accuracy of 0.3%, 3σ , for a determination of a 25-dB change in power levels. The Z_0 available power at the transmitter reference flange was determined to be +19.746 dB above full-scale indication of the instrument. A second RF head also of improved thermal design was used as a monitor

**Table 11. Measured off-source system noise temperatures
8448 MHz, DSS-13, XCE feedcone**

Elevation, deg	Average T_{SA} , °K	Standard deviation, °K
82	36.53	0.45
74	36.78	0.43
64	37.14	0.61
57	37.18	0.57
46	38.52	0.54
35	39.84	0.93
25	41.95	1.92
16	47.04	3.62
9	51.38	—

to detect possible long-term drifts in the carefully calibrated output. Because a separate amplitude levelling feedback loop was used, no drift more than a few millidecibels was detected for several hours in the transmitter output.

The calibrated portable bridge was then transported to the Venus station and attached to the maser reference flange within the XCE feedcone. Propagation conditions over the Tiefort-Venus path are seldom stable; however, during the gain test peak-to-peak fluctuations were about 0.5 dB, which, although considered acceptable, may be interpreted as partial decorrelation of the received wavefront. By use of a 10-s integrating DVM, the fluctuations were averaged and the mean received power at bore-sight was determined by dc substitution to be 24.587 dB below full-scale indication of the instrument, or approximately -14.6 dBm. This power level is sufficiently above instrumental jitter and drifts such that these defects are negligible.

Table 12 shows measured and computed parameters used in obtaining the gain using ground-based techniques. It is clear that further effort towards improving tolerances should be devoted to the gain standard horn calibration. Other possible sources of error, including multipath, polarization mismatch, antenna pointing, and possible wavefront decorrelation are considered small in comparison to the gain standard horn calibration error.

Because a dissipation loss of 0.150 dB occurs before the maser reference flange within the XCE feedcone, it is of interest to compare the measured aperture efficiency with the predicted, referenced to the antenna reference flange. Unfortunately, our knowledge of the surface tol-

**Table 12. Measured and computed parameters
ground-based gain measurement**

Parameter	Value	3 σ tolerance	Comment
Transmitter power at transmitter reference flange	+19.746 dB ref ^a	± 0.030 dB ^b	By dc substitution
Insertion loss, transmitter reference flange to aperture	-0.089 dB	± 0.060 dB	Estimated
Gain standard horn directivity	+29.510 dB	± 0.450 dB	Pattern integration, estimated
Effective radiated power	+49.187 dB ref	—	—
Path loss, Venus to Tiefort	-137.226 dB	± 0.039 dB	Inverse square, estimated
Path absorption, Venus to Tiefort	-0.165 dB	± 0.060 dB	Theoretical ^c
Expected received power for isotropic aperture	-88.204 dB ref	—	—
Received power level at maser reference flange	-24.587 dB ref	± 0.030 dB	By dc substitution
Observed gain G	+63.617 dB/isotropic	± 0.462 dB	At maser reference flange
Near-field correction	0.095 dB	± 0.095 dB	—
Far-field gain G_0	+63.712 dB	± 0.474 dB	At maser reference flange
Gain for 100% η	+67.210 dB	—	—
Efficiency at maser reference flange	(-3.498 \pm 0.474) dB, 3 σ	(44.69 \pm 4.89)%, 3 σ	
^a Reference is 10 mW, nominal. ^b Includes mismatch error. ^c Based on 0.89 atmospheric pressure, 20°C and 4 g/m ³ H ₂ O vapor (Ref. 15).			

erance, as discussed, is limited. We can, however, separate components of the efficiency and solve for the effective system surface tolerance at the elevation angle of the collimation station. Table 13 shows the method;

CALB
ERR CRDS

CALB
TAGC

1 9.9269660
2 2.0283544
3 .0174448
4 -.0040864
5 .0001373

AGCV	DBM	Y	Y-DBM
.035	-100.000	-99.988	.01160
.157	-101.000	-101.052	.05196
.264	-102.000	-101.969	.03124
.384	-103.000	-102.975	.02505
.757	-106.000	-105.957	.04287
1.153	-109.000	-108.928	.07190
1.601	-112.000	-112.067	.06660
2.058	-115.000	-115.048	.04833
2.556	-118.000	-118.079	.07860
3.079	-121.000	-121.032	.03244
3.658	-124.000	-124.067	.06659
4.254	-127.000	-126.956	.04439
4.901	-130.000	-129.852	.14792
5.653	-133.000	-132.946	.05447
6.444	-136.000	-135.916	.08390
7.382	-139.000	-139.120	.12011
8.344	-142.000	-142.091	.09057
9.445	-145.000	-145.163	.16327
10.436	-148.000	-147.680	.31954
11.476	-150.000	-150.115	.11502

CURVE FIT ERROR # .107 DBM RMS

Fig. 25. Polynomial curve fit computation for radiation patterns

Table 13. Effective system surface tolerance computation

Parameter	Efficiency	1 σ tolerance	Comment
Aperture integration	0.7388	± 0.002	Estimated
Quadripod blocking	0.8755	± 0.008	80 to 120% opacity times physical area
Measured	0.4626	± 0.0163	At antenna reference flange
Balance	0.7152	± 0.0141	
Effective system surface tolerance in rms in. at 0.8 deg elevation	0.065	± 0.002	

the efficiency balance of 0.715 is all attributed to the Ruze type of loss, which leads to 0.065 in. rms.

Radiation patterns of the system were taken using the high-level AGC radiometer. The collimation tower signal was attenuated in discrete steps, AGC voltages were recorded and entered into a polynomial curve fit program. Figure 25 shows the computed coefficients, the input data, and the residuals after fitting. A peak residual of 0.3 dB was obtained using this method. Figure 26 shows the fitted AGC curve. Azimuth and elevation scans were made over ± 0.5 deg at a rate of 0.003 deg/s with the

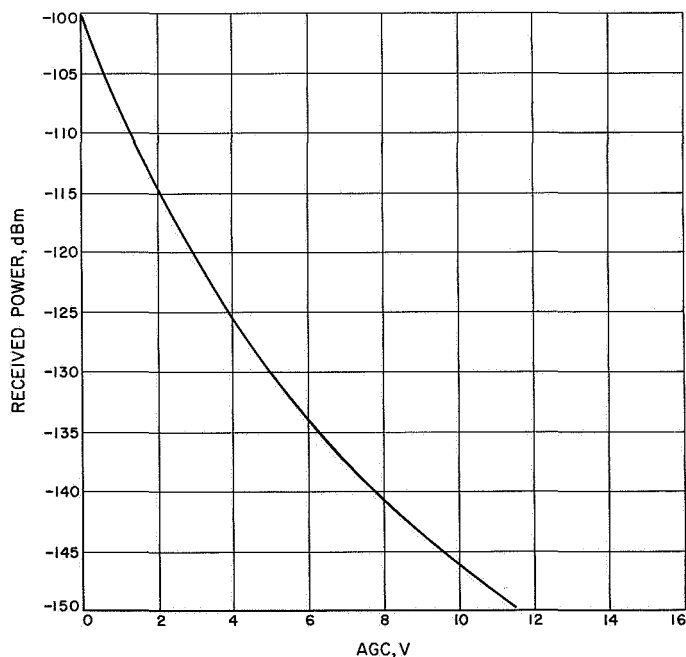


Fig. 26. Polynomial curve for radiation patterns

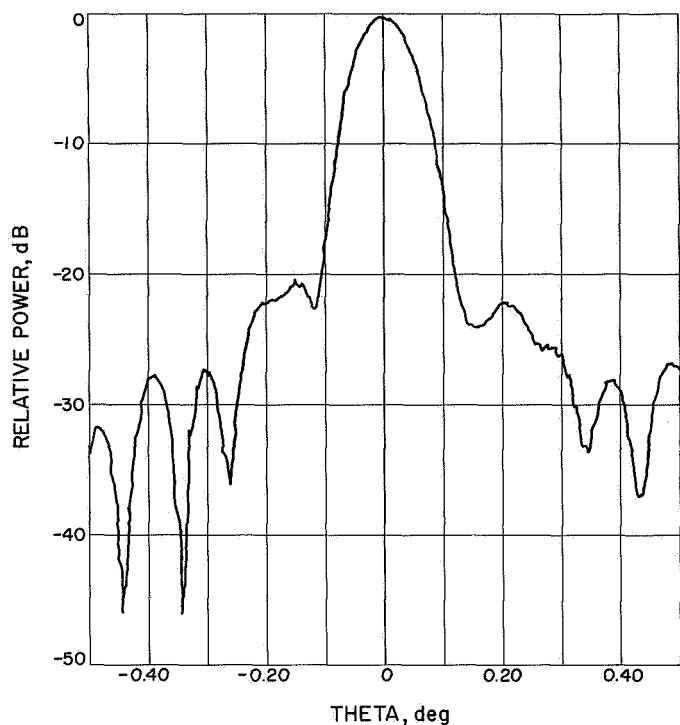


Fig. 27. Radiation pattern, 85-ft az-el reflector, near-field focus, azimuth

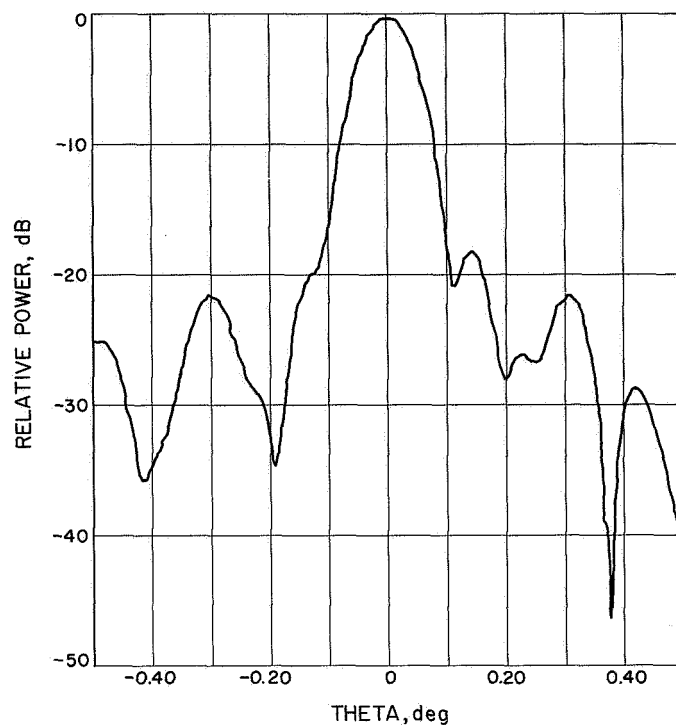


Fig. 28. Radiation pattern, 85-ft az-el reflector, near-field focus, elevation

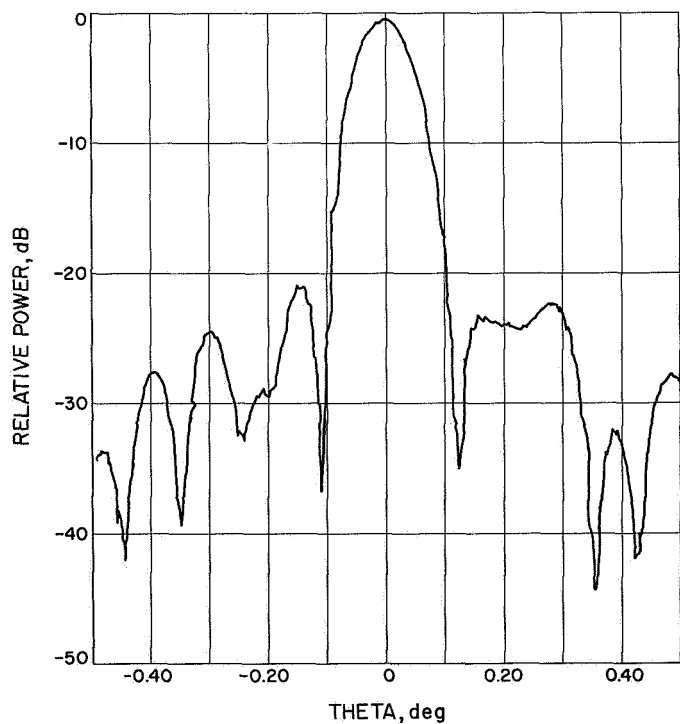


Fig. 29. Radiation pattern, 85-ft az-el reflector, near-field source at horizon, focused for high-elevation-angle peak gain, azimuth

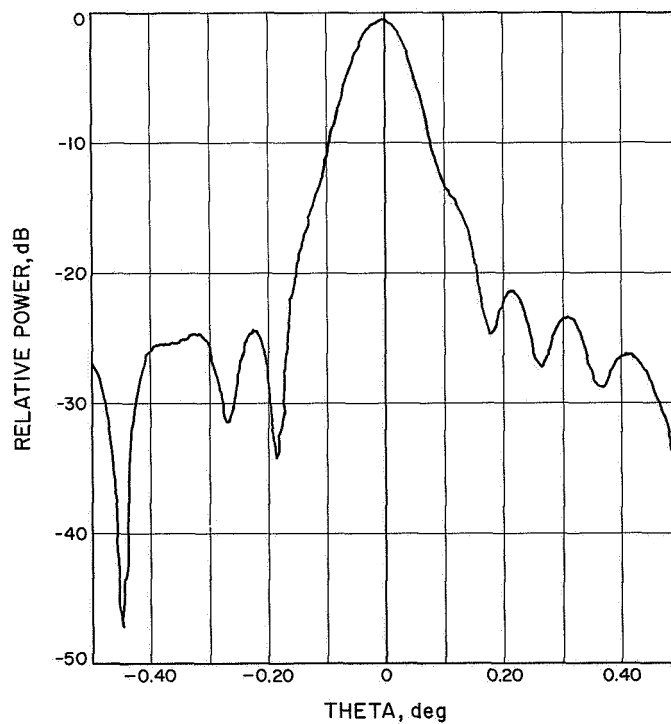


Fig. 30. Radiation pattern, 85-ft az-el reflector, near-field source at horizon, focused for high-elevation-angle peak gain, elevation

station digitizing equipment sampling once per second and preparing punched tapes. The tapes were later played back and plotted. Figures 27 and 28 show the patterns taken at a hyperboloid focus adjusted for optimum gain on the somewhat near-field source. Each pattern requires a 5-min scan which is a long period compared with the small amplitude scintillations present. Some evidence of the scintillations is present in Figs. 27 and 28. Qualitatively the patterns show a reasonably well-formed beam is produced with a half-power beam-width less than 0.100 deg in both planes.

Figures 27 and 28 may be compared with the computed patterns given in Section V for 1× and 3× deflection cases, since the computed patterns account for the near-field source. It is clear that patterns obtained with the 1× computed deflection data do not agree with the actual behavior. Patterns obtained with 3× computed deflections, resulting in a paraboloid rms of 0.074 in. (Table 10) more nearly fit the experimental.

The hyperboloid was then set 0.500 in. toward the apex, which approximates the high elevation angle focus for maximum gain. Figures 29 and 30 show the resultant patterns. The azimuth cut is seen to have a narrower main beam while the elevation cut is broader. This effect is indicative that the optimum gain position of the hyperboloid near the horizon is fitting different azimuth and elevation plane focal lengths. Although a corresponding hyperboloid position toward the vertex was not tried, it is suspected the inverse would be true, i.e., the elevation plane would be nearer an optimum focus and the azimuth plane would be defocused.

The difficulty in extending the ground-based efficiency value to higher elevation angles for the purpose of a direct determination of the Cygnus flux can be seen in Fig. 31, which relates surface efficiency to surface tolerance for 8448 MHz. It is clear that a very small change in the effective system surface tolerance will cause an appreciable change in system efficiency. The fact that the system was operated in a fix-focused manner compounds the difficulty.

For purposes of possible future work toward radio astronomical flux determination referenced to a ground based gain measurement, it is recommended the focusing be implemented in a convenient manner to keep the antenna gain peaked, at least for the large-aperture high-frequency domain considered in this report.

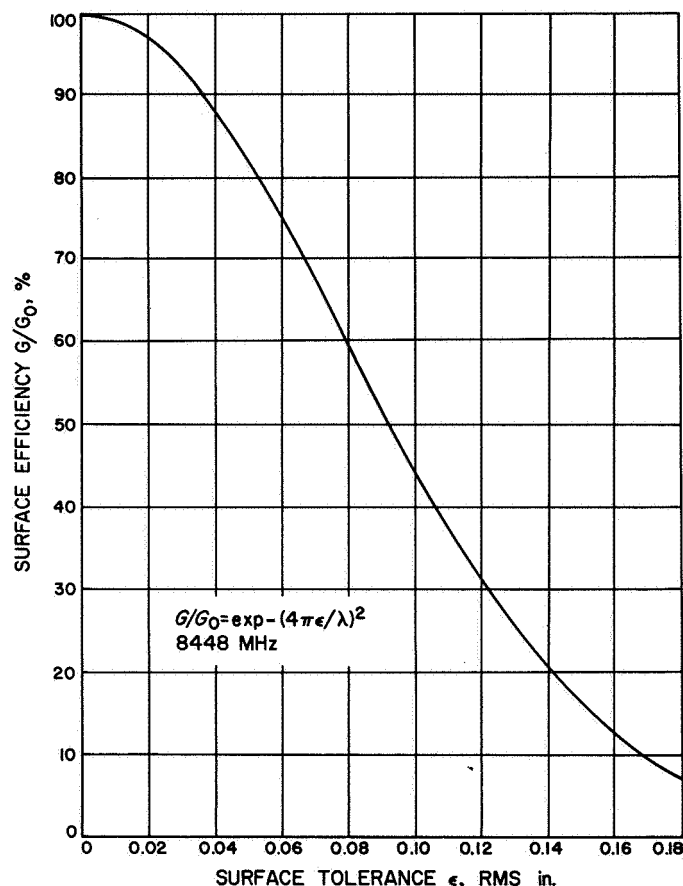


Fig. 31. Surface efficiency as a function of surface tolerance, 8448 MHz

VII. Conclusion

An 85-ft diameter paraboloid aperture efficiency at X-band has been evaluated by independent methods; the results are in good agreement. Based on a selected value of flux density for Cygnus A, efficiency as a function of elevation angle has been obtained, and based on an independent ground-based method the efficiency near 1 deg elevation angle has been measured. Table 14 gives the final results. Although the mean values are consistent

Table 14. Independent methods of efficiency determination

Method	Efficiency at maser reference flange	Comment
Radio astronomical	$(46.2 \pm 11.1)\%$, 3σ	Applicable for 40–70 deg elevation
Ground-based	$(44.7 \pm 4.9)\%$, 3σ	Applicable for 0.8 deg elevation

with expectations of a better system surface tolerance at high elevation angles (the surface was originally set optimally at 45 deg elevation angle), it is felt further analysis is unwarrantable.

An rms-to-diameter precision index, $\epsilon/D \sim 0.7 \times 10^{-4}$ for all conditions encountered, places the X-band work always below $0.6 \times$ gain limit frequency.

The X-band evaluation described was conducted with no particular concern for weather conditions. No rain occurred during the tests but occasional moderate cloudiness and humidity were noted. Wind, which is common in the high-desert area, ranged to 45 mph. The philosophy adopted was that of obtaining, under nonselected conditions, performance data on a system possibly useful for specialized deep space communications.

References

1. Potter, P. D., Merrick, W. D., and Ludwig, A. C., *Large Antenna Apertures and Arrays for Deep Space Communications*, Technical Report 32-848. Jet Propulsion Laboratory, Pasadena, Calif., Nov. 1, 1965.
2. Potter, P. D., *The Design of a Very High Power, Very Low Noise Cassegrain Feed System for a Planetary Radar*, Technical Report 32-653. Jet Propulsion Laboratory, Pasadena, Calif., Aug. 24, 1964.
3. Rusch, W. V. T., "Scattering from a Hyperboloidal Reflector in a Cassegrainian Feed System," *IEEE Transactions on Antennas and Propagation*, Volume AP-11, No. 4, pp. 414-421, July 1963.
4. Rusch, W. V. T., "Phase Error and Associated Cross-Polarization Effects in Cassegrainian-Fed Microwave Antennas," *IEEE Transactions on Antennas and Propagation*, Volume AP-14, No. 3, pp. 266-275, May 1966.
5. Ludwig, A. C., "Antenna Feed Efficiency," in *Space Programs Summary 37-26*, Vol. IV, pp. 200-208. Jet Propulsion Laboratory, Pasadena, Calif., April 30, 1964. (See also A. C. Ludwig, "Antenna Feed Efficiency," in *Computer Programs for Antenna Feed System Design and Analysis. Volume I: Programs and Sample Cases*, Technical Report 32-979, pp. 69-71. Edited by A. Ludwig. Jet Propulsion Laboratory, Pasadena, Calif., April 15, 1967.
6. Ludwig, A. C., "Efficient Antenna Systems: Aperture Blockage and Surface Tolerance Loss Calculations for Non-Uniform Illumination and Error Distribution," in *Space Programs Summary 37-41*, Vol. III, pp. 89-90. Jet Propulsion Laboratory, Pasadena, Calif., Sept. 30, 1966.
7. Petty, S. M., and Clauss, R. C., "X-Band Traveling Wave Maser," *IEEE Transactions on Microwave Theory and Techniques*, Vol. MTT-16, No. 1, pp. 47-48, Jan. 1968.
8. Lastochkin, V. P., Sorin, Yu. M., and Stankevich, K. S., "Spectrum of Radio Emission from Cygnus A," *Soviet Astronomy-A. J.*, Vol. 8, No. 4, pp. 613-614, Jan.-Feb. 1965.
9. *Microwave Antenna Theory and Design*, pp. 196-199. Edited by S. Silver. McGraw-Hill Book Co., Inc., 1949.

References (contd)

10. Bathker, D. A., "Radiation Pattern Programs," in *Computer Programs for Antenna Feed System Design and Analysis. Volume I: Programs and Sample Cases*, Technical Report 32-979, pp. 107-110. Edited by A. Ludwig. Jet Propulsion Laboratory, Pasadena, Calif., April 15, 1967.
11. Ludwig, A. C., "Gain Computations from Pattern Integration," *IEEE Transactions on Antennas and Propagation*, Vol. AP-15, No. 2, pp. 309-311, March 1967.
12. Katow, M. S., and Schmele, L., "Utku/Schmele Paraboloid RMS Best-Fit Program," in *Computer Programs for Antenna Feed System Design and Analysis. Volume I: Programs and Sample Cases*, Technical Report 32-979, pp. 75-82. Edited by A. Ludwig. Jet Propulsion Laboratory, Pasadena, Calif., April 15, 1967.
13. Katow, M. S., Bartos, K. P., and Matsumoto, R., *JPL Modified STAIR System Operating Procedures*, Technical Memorandum 33-304. Jet Propulsion Laboratory, Pasadena, Calif., May 1968.
14. Katow, M. S., "85-ft Az-El Antenna Structure Deformations From Gravity Loads," in *Space Programs Summary 37-44*, Vol. III, pp. 106-110. Jet Propulsion Laboratory, Pasadena, Calif., March 31, 1967.
15. Bean, B. R., and Dutton, E. J., *Radio Meteorology*, U.S. Department of Commerce, National Bureau of Standards Monograph 92, March 1, 1966.